GEOSPHERE

GEOSPHERE, v. 18, no. 2

https://doi.org/10.1130/GES02367.1

9 figures

CORRESPONDENCE: jacob.geersen@ifg.uni-kiel.de

CITATION: Geersen, J., Sippl, C., and Harmon, N., 2022, Impact of bending-related faulting and oceanic-plate topography on slab hydration and intermediate-depth seismicity: Geosphere, v. 18, no. 2, p. 562–584, https://doi.org/10.1130/GES02367.1.

Science Editor: Shanaka de Silva
Guest Associate Editor: Philippe Agard

Received 16 November 2020
Revision received 13 August 2021
Accepted 5 November 2021

Published online 17 February 2022

Impact of bending-related faulting and oceanic-plate topography on slab hydration and intermediate-depth seismicity

Jacob Geersen[1,*], Christian Sippl[2], and Nicholas Harmon[3]

[1]GEOMAR Helmholtz Centre for Ocean Research Kiel, Wischhofstraße 1-3, 24148 Kiel, Germany
[2]Institute of Geophysics, Czech Academy of Sciences, Boční II/1401, 141 31 Praha –Spořilov, Czech Republic
[3]Ocean and Earth Science, National Oceanography Centre Southampton, University of Southampton Waterfront Campus, European Way, Southampton SO14 3ZH, UK

ABSTRACT

It is commonly assumed that intermediate-depth seismicity is in some way linked to dehydration reactions inside subducting oceanic plates. Although there is growing evidence that the hydration state of an oceanic plate is controlled by its structure and degree of faulting, we do not have a quantitative understanding of this relationship. Double seismic zones offer the possibility of investigating changes in oceanic-plate hydration not only along strike but also with depth beneath the slab surface. To quantify the impact of oceanic-plate structure and faulting on slab hydration and intermediate-depth seismicity, with a focus on the genesis of double seismic zones, we correlate high-resolution earthquake catalogs and seafloor maps of ship-based bathymetry for the northern Chilean and Japan Trench subduction zones. The correlations show only a weak influence of oceanic-plate structure and faulting on seismicity on the upper plane of the double seismic zone, which may imply that hydration is limited by slow reaction kinetics at low temperatures 5–7 km below the seafloor and by the finite amount of exposed wall rock in the outer-rise region. These factors seem to limit hydration even if abundant water is available. Seismicity in the lower plane is, in contrast, substantially enhanced where deformation of the oceanic plate is high and distributed across intersecting faults. This likely leads to an increase in the volume of damaged wall rock around the faults, thereby promoting the circulation of water to mantle depths where serpentinization is faster due to elevated temperatures. Increased lower-plane seismicity around subducting oceanic features such as seamounts or fracture zones may also be caused by enhanced faulting around these features. Our results provide a possible explanation for the globally observed presence of rather homogeneous upper-plane seismicity in double seismic zones as well as for the commonly patchy and inhomogeneous distribution of lower-plane seismicity.

INTRODUCTION

Subduction zones are among the least understood parts of the global water cycle. It is generally accepted that subducting oceanic plates carry substantial amounts of water, which is partly released during the slab's descent into the mantle (Rüpke et al., 2004; Hacker, 2008; van Keken et al., 2011). Transform faults, basement outcrops such as seamounts or magmatic ridges, as well as oceanic fracture zones can act as conduits for fluids into an oceanic plate (Wolery and Sleep, 1976; Klügel et al., 2011; Faccenda, 2014; Cooper et al., 2020). At the trench and outer-rise region of subduction zones, bending-related normal faults allow fluids to hydrate the crust and upper mantle (Ranero et al., 2003). It has been proposed that the degree and depth extent of plate hydration at the outer rise is controlled by the magnitude of tectonic faulting (Ranero et al., 2003, 2005; Boneh et al., 2019). There are doubts about whether outer-rise normal faulting is capable of promoting substantial deep hydration within the oceanic mantle (e.g., Korenaga, 2017). However, recent observations of severely lowered shear-wave velocities to depths of ≥25 km at the Mariana outer rise (Cai et al., 2018) appear to provide direct evidence for deep hydration at the outer rise. Moreover, reaction-induced fracturing provides a plausible physical mechanism for mantle serpentinization that could operate in outer-rise regions (Plümper et al., 2012).

At shallow depth in a subduction zone (<10 km), the dominant processes that liberate water are assumed to be compaction dewatering and clay and opal dehydration reactions in subducting sediments and the upper oceanic basement (Saffer and Tobin, 2011). While this water usually gets dispelled beneath the accretionary prism or outermost forearc, water contained in the middle and lower oceanic crust and uppermost mantle is bound in more stable hydrous minerals. The most prominent such mineral phases are amphibole and lawsonite for basalt and gabbro, and different variants of serpentinite for peridotitic mantle. Beyond those, there is a large variety of additional, commonly exotic, mineral phases capable of transporting water to depth (for oceanic crust, cf. Ono, 1998; for mantle, cf. Ferrand, 2019). Water bound in the crystal lattice of such minerals is retained to high pressures and high temperatures and only gets liberated when pressure and temperature (*P-T*) conditions that promote phase transformations of the hydrous minerals are reached.

Intermediate-depth earthquakes (i.e., between 60 and 300 km) are commonly thought to be linked to dehydration processes in the subducting slab, although the exact mechanism of earthquake creation is still contentious (Yamasaki and Seno, 2003; Hacker et al., 2003; Kelemen and Hirth, 2007; Ferrand et al., 2017). From the geologic record of fossil subduction zones (e.g., Scambelluri et al., 2017) and from laboratory studies (thermal runaway

Jacob Geersen https://orcid.org/0000-0001-5625-493X
*Now at Institute of Geosciences, Kiel University, Otto-Hahn-Platz 1, 24118 Kiel, Germany

processes; Kelemen and Hirth, 2007; John et al., 2009), there is evidence that the genesis of intermediate-depth earthquakes is theoretically also possible under dry conditions. The observation that intermediate-depth seismicity usually occurs where dehydration reactions are expected inside subducting lithosphere (e.g., Hacker et al., 2003), however, suggests that these processes might not be dominant on a global scale. It is also discussed whether a combination of dehydration-related earthquake nucleation and rupture propagation via thermal runaway may provide an explanation for intermediate-depth seismicity (Zhan, 2020).

Ranero et al. (2005) documented a correlation between focal mechanisms of outer-rise earthquakes and intermediate-depth earthquakes for Central America and Chile and suggested a causal link. However, a similar interrelation seems to be absent along the Tonga-Kermadec subduction zone (Warren et al., 2007). Kirby et al. (1996) observed higher numbers of intermediate-depth earthquakes along the prolongations of first-order structural features like ridges and seamount chains for the South American margin. Double seismic zones, parallel arrangements of earthquake hypocenters along two planes following the slab dip but separated by 15–35 km, have been observed at many subduction zones in this depth interval (Brudzinski et al., 2007). Although several questions regarding the genesis of double seismic zones are still unanswered, it is generally accepted that their presence requires a hydrated subducting plate and possibly also the presence of a certain level of stress (Faccenda et al., 2012). The lower plane of double seismic zones is situated within the oceanic mantle lithosphere and has repeatedly been linked to the breakdown of antigorite serpentinite at temperatures of 600–650 °C (e.g., Peacock, 2001). For the upper plane of double seismic zones, it is not entirely clear whether earthquakes occur in the oceanic crust or the uppermost kilometers of the lithospheric mantle (Abers et al., 2013). In the crust, eclogitization of basaltic or gabbroic crustal rocks (Kita et al., 2006; Nakajima et al., 2013; Yuan et al., 2000) is the most commonly inferred mineral reaction, whereas in the uppermost lithospheric mantle, the dehydration of brucite or antigorite might be the main driver for upper-plane seismicity (e.g., Bloch et al., 2018a). While upper-plane seismicity tends to be rather homogeneously distributed along a given subduction segment, lower-plane earthquake occurrence is more variable, with tightly confined clusters and large aseismic areas (Igarashi et al., 2001; Sippl et al., 2018). This may indicate that while the subducting plate is largely homogenously hydrated at depths of 5–7 km beneath the slab surface, special conditions are necessary to allow hydration at depths of >25 km beneath the slab surface.

In this study, we examine the hypothesis that intermediate-depth earthquakes spatially coincide with the expected depth of dehydration reactions inside subducting slabs. We correlate the structure of the oceanic plate and the magnitude of tectonic faulting in the outer-rise region to the density of upper- and lower-plane earthquakes at intermediate depths. Using high-resolution earthquake catalogs that distinguish between upper- and lower-plane events, we can now obtain information about spatial variations in the magnitude and the depth of hydration along individual subduction zones. Correlating this information with the structure and deformation of the ocean floor at the respective outer rise allows us to evaluate whether regions of intense upper- and/or lower-plane seismicity have an identifiable ocean-floor signature farther updip. We perform this analysis for the Japan Trench and the northern Chile margin, the only regions where both seismicity and bathymetry data of sufficient resolution are available (Fig. 1).

DATA AND METHODS

Bathymetric Data

Detection and characterization of bending-related faults was conducted by means of shipborne bathymetric data. In the case of northern Chile (Fig. 2), we used the compilation provided by Geersen et al. (2018a), which includes data from German and U.S. research cruises as well as masked data from the Global Multi-Resolution Topography (GMRT) synthesis (Ryan et al., 2009). For the Japan Trench and marine forearc (Fig. 3), we collated bathymetric information from multiple research cruises accessed through the Data and Sample Research System for Whole Cruise Information (DARWIN) database (Japan Agency for Marine-Earth Science and Technology, 2016). The data from the Japanese cruises were complemented by the data provided by Geersen (2019), masked data from the GMRT synthesis (Ryan et al., 2009), and bathymetric data collected during R/V *SONNE* cruise SO251-1 (Strasser et al., 2017).

Fault Mapping and Characterization

For both margins, we used existing fault maps (Kobayashi et al., 1998; Nakanishi, 2011; Nakata et al., 2012; Geersen et al., 2018a), which were updated and extended based on the new collection of shipborne bathymetric data. The fault outcrops at the seafloor were digitized and stored in an ArcGIS database. To estimate fault activity throughout the study region, we calculated the mean elevation on both sides of the faults within 1-km-wide segments parallel to the fault trace. By multiplying the elevation difference for each fault with the length of the respective fault, we determined the exposed fault area, which we use as a proxy for fault activity. The derived exposed fault areas therefore represent average values for each fault and do not account for secondary effects such as localized erosion of the fault scarp or post-tectonic sedimentation. Fault strike directions were calculated in ArcGIS using the "linear direction mean" tool and plotted with the NetworkGT toolbox (Nyberg et al., 2018) (Fig. 4). This toolbox was also used to analyze the connectivity of the faults on the oceanic plate. The "branches and nodes" tool distinguishes between isolated faults, faults that crosscut other faults, and faults that abut (splay) from other faults. Isolated end points of faults are classified as I nodes, fault intersections are classified as X nodes, and splays are classified as Y nodes (Fig. 5) (cf. Sanderson and Nixon, 2015, 2018). Due to the local presence of

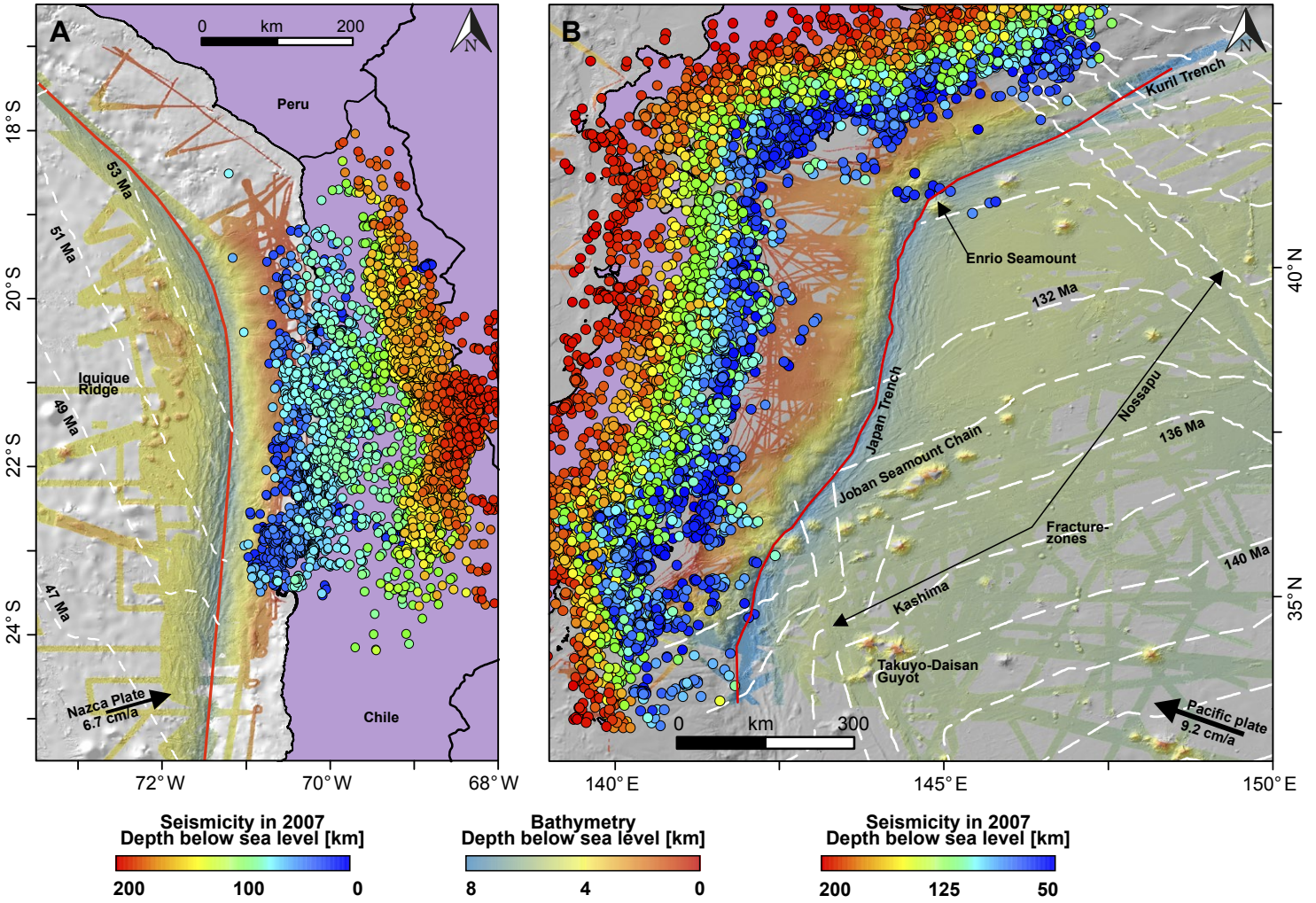

Figure 1. Bathymetric maps of the northern Chilean (A) and Japan Trench (B) subduction zones. White dashed lines mark isochrons of oceanic-plate age (Müller et al., 2008). Red line represents the deformation front. Colored dots show event locations and depths in 2007 from the earthquake catalogue of Sippl et al. (2018) for northern Chile and the Japan Meteorological Agency earthquake catalog (https://www.jma.go.jp/en/quake/) for Japan.

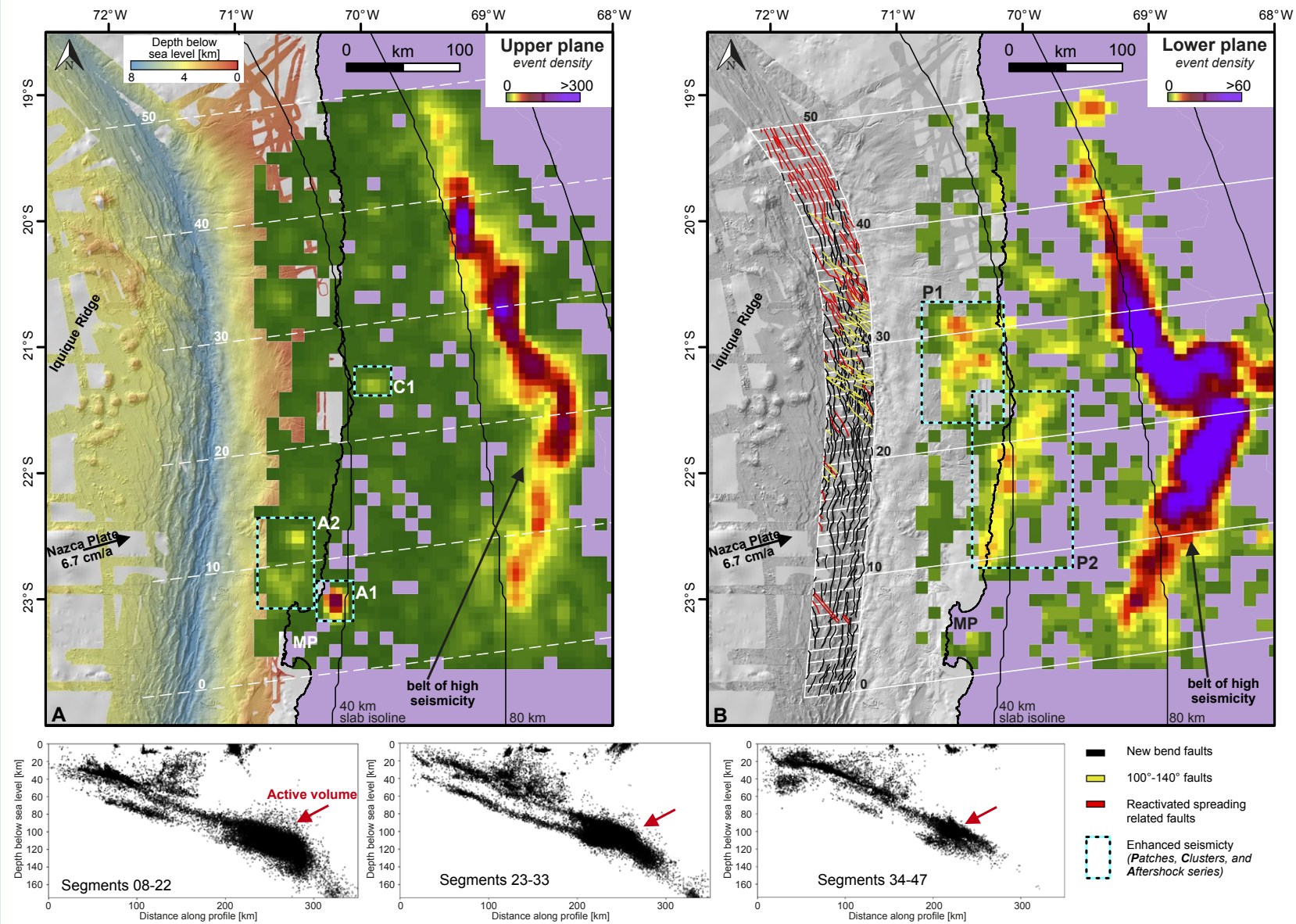

Figure 2. Spatial distribution of upper-plane (A) and lower-plane (B) seismicity on the double seismic zone in northern Chile between 2007 and 2017. Displayed are the number of events that occurred within a region of 30 km². Prominent seismicity features are outlined by the cyan boxes (A—aftershock series; C—cluster; P—patch) (cf. Fig. 7). White lines and numbers indicate selected boundaries between 10-km-wide segments of the oceanic plate that were introduced to group the tectonic observations (cf. Figs. 5–6). Curved black lines are slab-surface isolines at 40, 80, and 120 km depth. Panel A shows the color-coded depth to the seafloor, whereas panel B shows a line drawing of oceanic-plate faults in the trench and outer-rise region on top of the shaded-relief bathymetric map. Faults that are oriented parallel (within a range of 30°) to the paleo-spreading fabric are highlighted by red lines, whereas new bend faults are shown by black lines; yellow lines represent faults striking 100°–140°, which is oblique to the paleo-spreading fabric and oblique to the trend of the trench and coastline. Three figures at the bottom show the along-dip location of earthquakes for selected segments over the entire observation period (2007–2017). MP—Mejillones Peninsula.

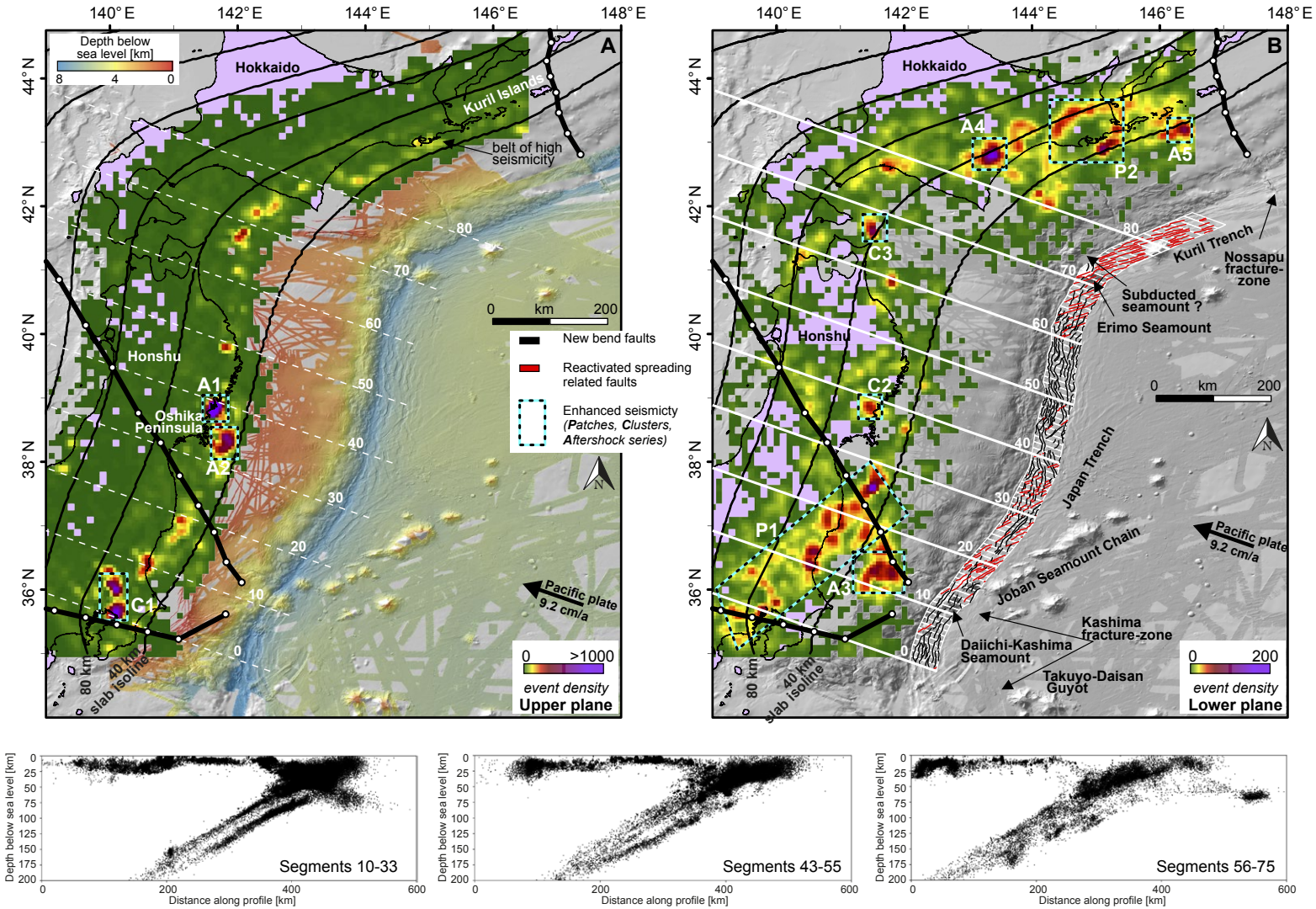

Figure 3. Spatial distribution of upper-plane (A) and lower-plane (B) seismicity on the double seismic zone in the Japan Trench subduction zone between 2000 and 2017. Displayed are the number of events that occurred within a region of 30 km². Black lines with white dots are the projections of the Joban Seamount Chain and the Kashima and Nossapu fracture zones onto the subducting slab. Prominent seismicity features are outlined by the cyan boxes (A—aftershock series; C—cluster; P—patch) (cf. Fig. 7). White lines and numbers indicate selected boundaries between 10-km-wide segments of the oceanic plate that were introduced to group the tectonic observations (cf. Figs. 5–6). Curved black lines are slab-surface isolines at 40, 80, 120, 160, 200, and 240 km depth. Panel A shows the color-coded depth to the seafloor, whereas panel B shows a line drawing of oceanic-plate faults in the trench and outer-rise region on top of the shaded-relief bathymetric map. Faults that are oriented parallel (within a range of 30°) to the paleo-spreading fabric are highlighted by red lines, whereas new bend faults are shown by black lines. Three figures at the bottom show the along-dip location of earthquakes for selected segments over the entire observation period (2000–2017).

some trench sediments (especially in the Japan Trench), it was not always possible to map the surface outcrops of intersecting faults on both sides of the intersection. Because in these cases it is unclear whether the fault intersection forms an X or a Y node, we group X and Y nodes and only distinguish between isolated faults (I nodes) and intersecting faults (X nodes and Y nodes). To systematically quantify spatial changes in oceanic-plate faulting, we introduced 10-km-wide oceanic-plate segments that strike in the direction of plate convergence (Figs. 2–3). The segments start at the deformation front and extend 40 km onto the oceanic plate. For each segment, we summed up the cumulative fault length and the cumulative exposed fault area for groups of faults with different strike directions. We further analyzed the number of I nodes as well as X and Y nodes for each segment.

Seismicity

Spatially variable detection rates of earthquakes due to non-homogeneous network distribution can severely skew earthquake numbers in seismicity catalogs. Areas with a lower detection threshold will commonly appear to be particularly active, whether or not this is actually the case. To overcome this limitation, we discarded all events below a magnitude of completeness (M_c; see, e.g., Wiemer and Wyss, 2000), above which the catalogs are assumed to not lack any events.

For the northern Chilean margin, we analyzed an earthquake catalog that is an extension of the catalog of Sippl et al. (2018) and contains 130,840 events from the time period 2007–2017. Event classifications into upper plate, plate

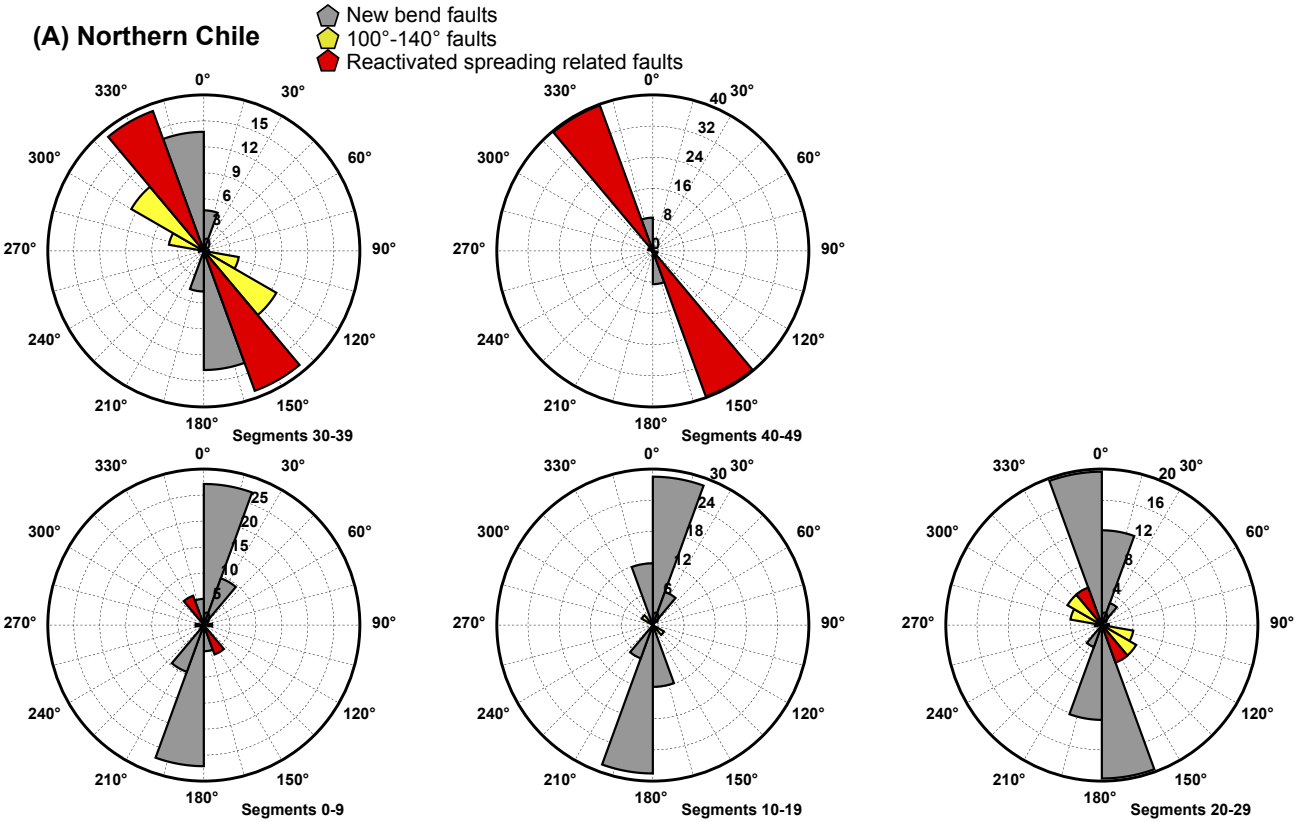

Figure 4. Rose diagrams of fault orientations for the northern Chilean (A) and Japan Trench (B) subduction zones. Red indicates reactivated spreading related faults; gray, new bend faults; yellow, faults striking 100°–140°, which is oblique to the paleo-spreading fabric and oblique to the trend of the trench and coastline (Chile only). (***Continued on following page***).

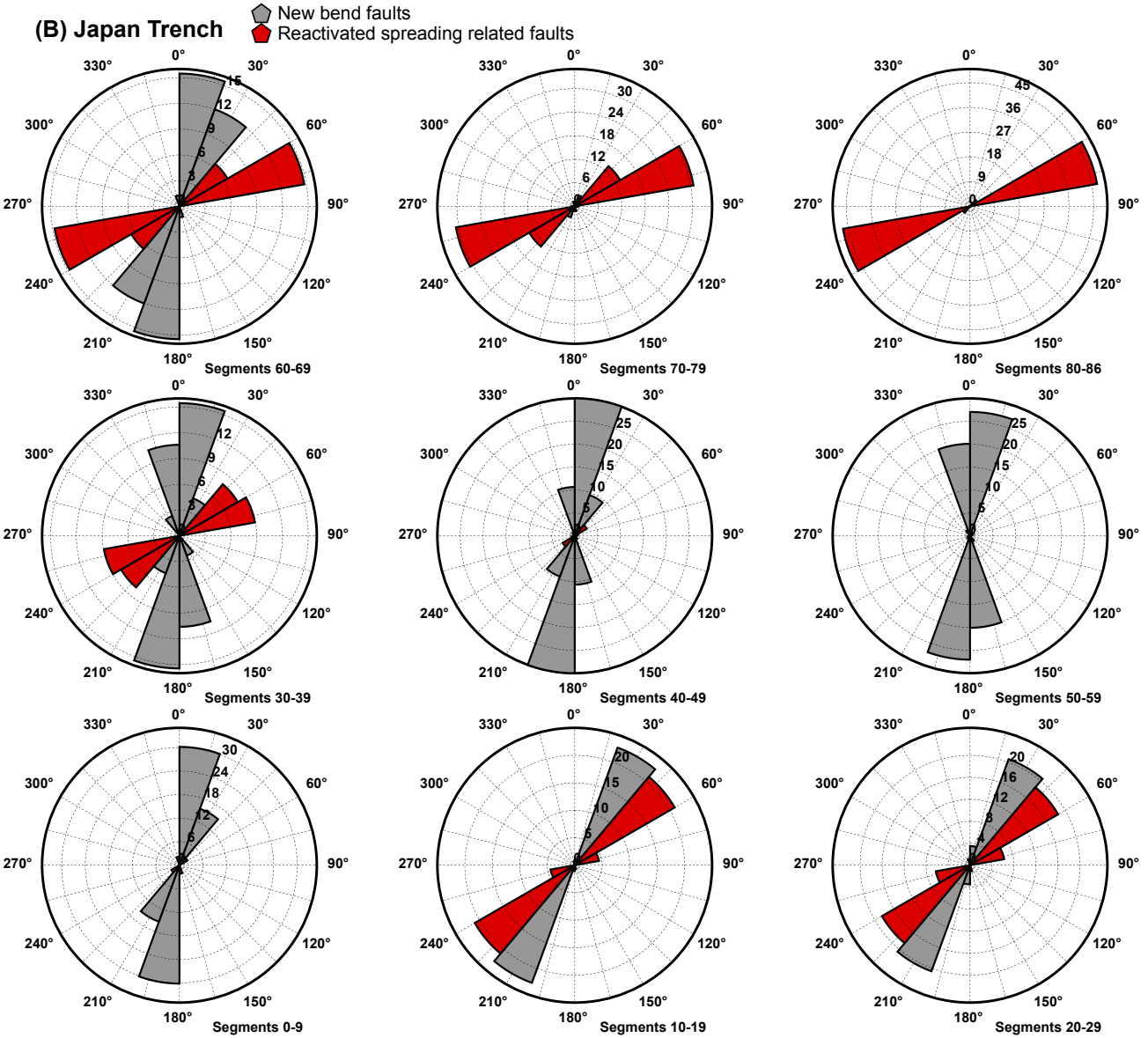

Figure 4 (*continued*). Orientations are organized into groups of 10 oceanic-plate segments (each segment is 10 km wide and strikes in the direction of plate convergence; see Figs. 2 and 3). Red indicates reactivated spreading related faults; gray, new bend faults; yellow, faults striking 100°–140°, which is oblique to the paleo-spreading fabric and oblique to the trend of the trench and coastline (Chile only).

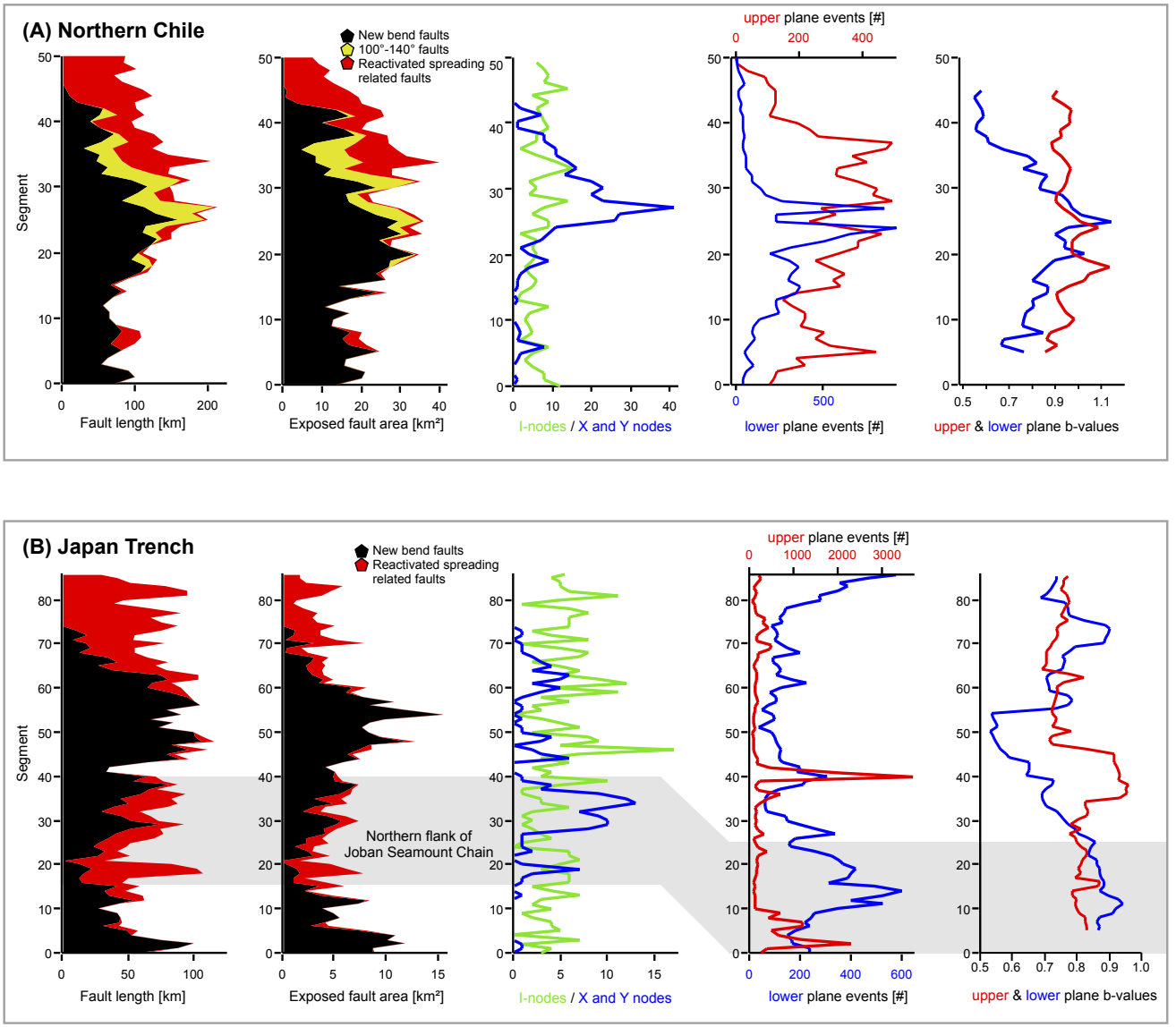

Figure 5. Statistical evaluation of fault length, exposed fault area, fault intersections, seismicity, and Gutenberg-Richter *b*-values per oceanic-plate segment (see Figs. 2–3) for double seismic zones at the northern Chilean (A) and Japan Trench (B) subduction zones. Graphs in the second column from the right show the number of upper- and lower-plane events for each segment projected into the subduction zone. The high number of lower-plane events at the northeastern tip of the Japan Trench subduction zone (segment numbers >75) is an artifact of the oblique (with respect to the coastline) trend of the segments. For the *b*-value curves (rightmost columns), the value for each segment represents an 11-segment window centered on the nominal segment (i.e., five segments in each direction). In the two leftmost columns, red indicates reactivated spreading related faults; black, new bend faults; yellow, faults striking 100°–140°, which is oblique to the paleo-spreading fabric and oblique to the trend of the trench and coastline (Chile only). Exposed fault areas were derived by multiplying the mean elevation difference on both sides of a fault with the length of the respective fault. Fault length and exposed fault area graphs are stacked.

interface, upper plane, lower plane, and deep volume are provided with the catalog (for specifics on how these are obtained, refer to Sippl et al. [2018]). The catalog contains 5806 events that are classified as upper plane and 3650 events in the lower plane. Downdip from a slab surface depth of ~80 km, the seismicity geometry changes and the planes can no longer be distinguished. Events from this ~25–30-km-thick volume at depths of 80–120 km (analyzed in detail in Sippl et al. [2019]) were classified independently. For the analysis presented in Figures 2 and 5, we added those events in this volume that occurred in the uppermost 10 km of the slab to the upper plane, and those that occurred at levels deeper than 20 km below the slab surface to the lower plane. Location uncertainties in the catalog are <5 km in the vertical direction (Sippl et al., 2019), which implies that only very few events might be misclassified between upper or lower plane. The M_c of the earthquake catalog was estimated as 2.7 (Hainzl et al., 2019).

For northeastern Japan, we analyzed the Japan Meteorological Agency (JMA) earthquake catalog (https://www.jma.go.jp/en/quake/) for the years 2000–2017. This catalog contains 2,734,452 events for all of Japan. We limited our analysis to earthquakes along the Japan Trench (latitudes 34.5°–45°N, longitudes 138°–146.5°E). Because no event classification into upper plate, upper plane, lower plane, and plate interface is supplied with the JMA catalog, and because it is commonly hard to separate the upper plane from the plate interface, we limited our analysis to earthquakes with hypocenters deeper than 50 km. This exceeds upper-plate thickness around Japan (generally <40 km; see Katsumata, 2010) and therefore should remove all plate-interface seismicity from the catalog. The remaining number of earthquakes after these restrictions is 237,941. The dip angle of slab seismicity in the JMA catalog is markedly different from the slab-surface geometry given in the Slab2 model (Hayes et al., 2018), which is likely a consequence of using a one-dimensional velocity model for hypocenter location. To separate upper and lower plane, we thus handpicked a plane that separates these different populations on a series of narrowly spaced north-south and east-west profiles (Fig. 6A). The obtained points were linearly interpolated together with the trench location, where the plane was required to be located at a depth of 15 km. Events that were located above and below the resulting plane by <30 km (Figs. 6B, 6C) were classified as upper- and lower-plane events. This implies that the classification into upper- and lower-plane events does not rely on absolute distance from the slab surface. Because the distance between the two planes is ~25 km (Fig. 6), we believe that the total number of events that are wrongly assigned to one of the planes is negligible. For the catalog's M_c in the Japan Trench area, we made a conservative estimate of 1.5 based on the maps of Nanjo et al. (2010).

Both earthquake catalogs document seismicity over a time span of more than a decade (11 years for northern Chile, 18 years for Japan). While this is longer than what is analyzed in most comparable studies, it obviously does not account for a full seismic cycle. However, intraslab seismicity has been shown to be much more steady state than, for example, earthquake occurrence on the megathrust (e.g., Sippl et al., 2019). It is further contentious whether the moment release from intermediate-depth earthquakes is modulated by interplate processes at all (Bouchon et al., 2018). To account for temporal variations due to the occurrence of large intraslab events, we examine regions with enhanced seismicity in detail and divide them into aftershock series, patches, and clusters (Fig. 7). Aftershock series feature a prominent peak in seismicity after a large-magnitude main shock followed by a rapid decay of event numbers following Omori's law. Patches, in contrast, define broad regions (hundreds of square kilometers) of elevated seismicity rate that are persistently active over the entire observation period. Clusters are likewise characterized by persistent elevated seismicity rates that are stable in space and time but extend only over small areas (tens of square kilometers).

For both earthquake catalogs, we further estimated *b*-values by the slopes of cumulative semilog Gutenberg-Richter curves of magnitude frequency, taking into account only events with $M > M_c$. To illuminate possible along-strike changes in *b*-values while retaining large-enough event numbers to ensure robustness of results, we derived *b*-values for 11-segment moving windows. The results are shown in Figure 5 for the upper and lower planes of the northern Chile and Japan subduction zones.

Projection of Tectonic Features onto the Subducting Slab

The projection of large-scale features such as fracture zones and seamount chains onto the subducting slabs beneath Japan was performed following the kinematic approach from Harmon et al. (2019). The method determines the location of the tectonic features on the subducting slab by moving the feature down the slab interface using the convergence velocity. It requires an estimate of the projection of the feature along the surface of the Earth prior to subduction and its location relative to the trench and the slab interface. The method assumes that trench geometry and slab geometry have been stable for the past 15 m.y. To estimate the fracture-zone positions at the surface of the Earth prior to subduction, we used the plate-motion model of Matthews et al. (2016) and projected ridge "flowlines" near the transforms from the Pacific-Izanagi plate ridge system. For seamount chains, we used a great-circle fit to the trend of the seamounts. We used the slab interface and trench location from the Slab2 model for the Kurile slab (Hayes et al., 2018) and convergence rates and directions taken from the plate-motion model of Matthews et al. (2016) to determine the trench position back in time. We used a 0.5 m.y. time step for the projections.

We assessed the validity of the assumption of a stable trench and slab geometry by inspection of the Matthews et al. (2016) plate-motion model to verify (1) that the local trench geometry has been stable over the past 15 m.y., and (2) that the accelerations in the relative plate motions have been small. We used the second test for acceleration as a proxy for slab geometry changes assuming that changes in velocity result from changes in vertical motion of the slab and therefore shallowing and steepening of the slab dip. For the European-Pacific plate system in the region of interest along the Japan Trench, the trench geometry is stable except in the southernmost part of the study area, south of 35.5°S. Here the boundary is affected by the rotation of the Izu-Bonin

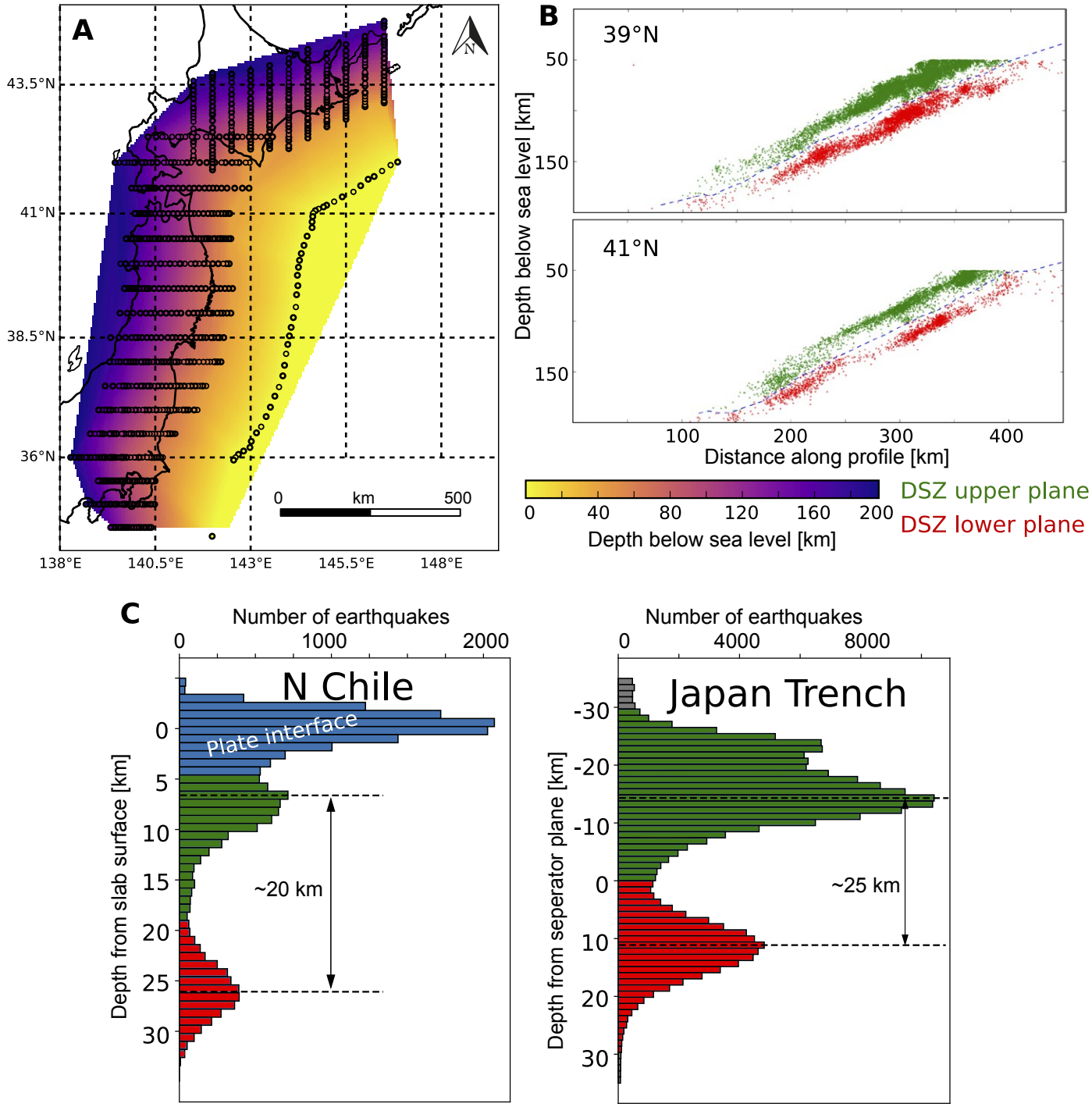

Figure 6. Implemented distinction between upper- and lower-plane seismicity in the double seismic zones (DSZs). Whereas the northern Chile catalog comes with labels for upper- and lower-plane events, we had to separate these ourselves for the Japan Meteorological Agency (JMA) catalog. (A) Separator plane between upper- and lower-plane events, hand-picked at 764 locations along 28 east-west or north-south profiles along the Japan Trench subducting slab, complemented by points located beneath the trench. Circles show the locations of individual depth picks. (B) Two examples of profiles through the JMA seismicity, with the separator plane shown as a blue dashed line. Seismicity classified as belonging to the upper plane is shown in green, lower plane in red. Note the depth cutoff at 50 km that we introduced so as to not erroneously include plate-interface events. (C) Histograms of earthquake depth relative to the slab surface (for northern Chile) or the separator plane (for Japan). Note the separation between upper- and lower-plane seismicity. Whereas plate-interface seismicity is also shown for northern Chile, it was removed by our depth cutoff for Japan.

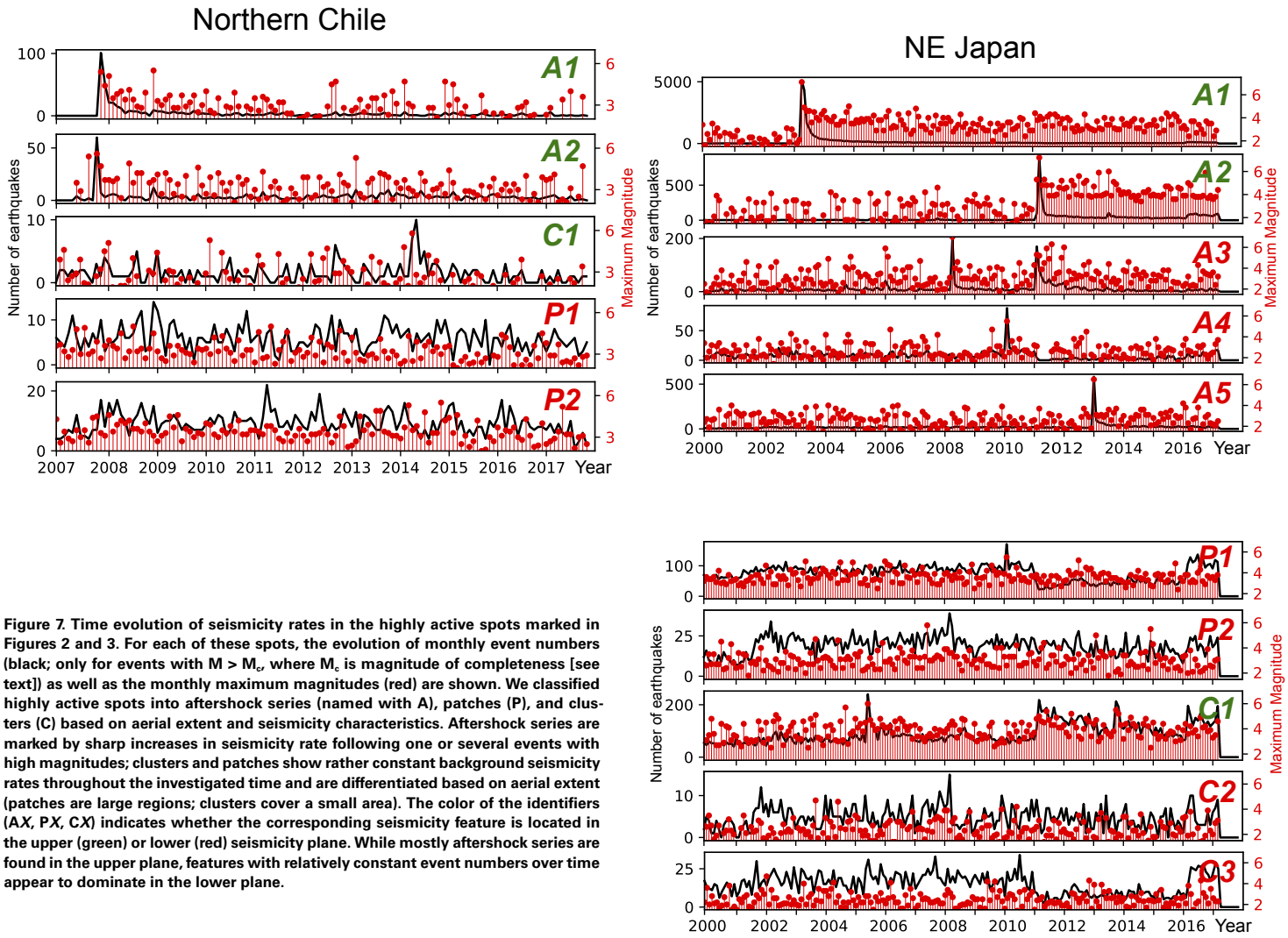

Figure 7. Time evolution of seismicity rates in the highly active spots marked in Figures 2 and 3. For each of these spots, the evolution of monthly event numbers (black; only for events with M > M_c, where M_c is magnitude of completeness [see text]) as well as the monthly maximum magnitudes (red) are shown. We classified highly active spots into aftershock series (named with A), patches (P), and clusters (C) based on aerial extent and seismicity characteristics. Aftershock series are marked by sharp increases in seismicity rate following one or several events with high magnitudes; clusters and patches show rather constant background seismicity rates throughout the investigated time and are differentiated based on aerial extent (patches are large regions; clusters cover a small area). The color of the identifiers (*AX*, *PX*, *CX*) indicates whether the corresponding seismicity feature is located in the upper (green) or lower (red) seismicity plane. While mostly aftershock series are found in the upper plane, features with relatively constant event numbers over time appear to dominate in the lower plane.

microplate. Accelerations for the European-Pacific plate system near the region of interest have also been small over the past 15 m.y., also <5 km/m.y. over a 2 m.y. period. Therefore, we believe the trench and slab geometries have been sufficiently stable to allow interpretation of our projections with confidence.

We did not project the Iquique Ridge onto the subducting Nazca slab. This is because the lack of ship-based bathymetric data seaward of the northern Chilean trench results in a high degree of uncertainty with respect to the trend of the ridge relative to the trench and the convergence direction. This trend, however, is the main parameter controlling the location of the subducted ridge at depths. Furthermore, the Iquique Ridge is flanked by a group of seamounts that seem to subduct into our study area and that may have a different genetic origin (and therefore trend on the oceanic plate) compared to the ridge.

NORTHERN CHILE

Geologic Setting of the Northern Chilean Subduction Zone

Along northern Chile, the Eocene oceanic Nazca plate subducts under the South American plate toward the east-northeast at a rate of ~7 cm/a (Fig. 2) (Angermann et al., 1999; Müller et al., 2008). The South American plate is substantially thickened in this area (crustal thickness ~60 km; Yuan et al., 2002), and has at least partially lost its mantle lithosphere beneath the Altiplano and Puna Plateaus east of the cordillera (Beck et al., 2015). With such a thick upper plate, the seismogenic zone of northern Chile extends to depths of ~55 km (Sippl et al., 2019), which hints at a relatively cold subduction setting.

The geometry of the subducted portion of the Nazca plate changes from a straight slab dipping at ~25° in the north (Dorbath et al., 2008) to a step-like pattern south of ~21°S where a flat section at ~80 km transitions into a steeper slab at larger depths (Sippl et al., 2018). The flattening likely increases farther southwards and transitions into the Pampean flat-slab section between 28°S and 32°S (Ramos et al., 2002). Slab seismicity shows a double seismic zone with ~20 km inter-plane spacing at depths of 45–80 km. Farther downdip, the double seismic zone changes into a 25-km-thick, highly active volume of earthquakes (Sippl et al., 2018; Fig. 2). Focal mechanisms in the upper and lower plane as well as in the highly active volume at depth show downdip extension, except in the upper plane where it is overlain by and thus likely mechanically coupled to the plate interface (Bloch et al., 2018b; Sippl et al., 2019).

Located adjacent to the hyper-arid Atacama Desert, the margin receives minimal terrestrial sediment influx and the trench is largely starved of sediment (Coulbourn and Moberly, 1977; Geersen et al., 2018a). This lack of sediment leads to a pristine preservation of tectonic structures on the oceanic Nazca plate, which are well documented in the morphology of the seafloor (Fig. 2). This setting offers a great opportunity for studying how the structure and deformation pattern of the oceanic plate changes along the margin. The Iquique Ridge represents the most prominent structural feature on the Nazca plate off northern Chile (Figs. 1–2). In the trench and outer-rise region, the ridge is located between ~20°S and ~22°S (Geersen et al., 2018a; Bello-González et al., 2018). It is flanked by multiple individual seamounts that are elevated as much as 1500 m from the surrounding seafloor (Geersen et al., 2018a). Geersen et al. (2015) further documented a series of subducting seamounts under the marine forearc, which may also be linked to the Iquique Ridge. Apart from the Iquique Ridge and the adjacent seamounts, there are no other first-order structural features such as fracture zones, hotspot tracks, or basement ridges that are currently colliding with the marine forearc. Although repeatedly described in a qualitative way (Moberly et al., 1982; von Huene et al., 1999; Sallarès and Ranero, 2005; Ranero et al., 2006; Geersen et al., 2015, 2018a, 2018b), spatial variations in oceanic plate faulting offshore northern Chile have not been quantified.

Oceanic-Plate Faulting off Northern Chile

Oceanic-plate faults in the trench and outer-rise region off northern Chile separate into three main strike directions (Fig. 4A). South of segment 23 (~21.7°S; Fig. 2), most faults strike parallel to the trench and coastline in a north-south direction (black lines in Fig. 2). Geersen et al. (2018a) interpreted these faults as extensional faults that newly developed after the oceanic plate started to bend. In contrast, north of segment 42 (~20°S), 140°–160° is the dominant strike direction (Fig. 4A). These faults (red lines in Fig. 2) likely represent the northwest-southeast–trending seafloor-spreading fabric formed at the mid-oceanic ridge. Striking <30° oblique to the trench and coastline, these faults are reactivated as extensional faults during plate bending (Ranero et al., 2005; Billen et al., 2007; Geersen et al., 2018a). A transition in strike direction occurs between 20°S and 21.7°S (segments ~23–42) where new bend faults and reactivated spreading related faults are both active. This transition zone, which coincides with the location of the Iquique Ridge in the trench and outer-rise region, is further shaped by a third fault group that strikes 100°–140° (yellow lines in Fig. 2; Fig. 4). This direction is oblique to both the trench and coastline as well as the paleo-spreading fabric. The two left graphs in Figure 5A show the stacked cumulative fault length and exposed fault area per segment for the three different fault groups. Both parameters are highest in the transition zone, where faults striking in multiple directions coexist in the vicinity of the Iquique Ridge.

The along-margin variations in strike direction result in a very distinct pattern with respect to the spatial distribution of I nodes on the one hand and X and Y nodes on the other hand (i.e., the distribution of isolated faults, crosscutting faults, and faults that abut from other faults). North of 20°S and south of 21.7°S, the almost exclusive presence of reactivated spreading-related faults (north) and new bend faults (south) leads to the dominance of I nodes. Here, faults that crosscut other faults are rare. In contrast, the transition zone between segments ~23 and 42 shows a high abundance of X and Y nodes, indicating the crosscutting relationship of new bend faults, reactivated spreading-related faults, and faults that strike 100°–140°.

Upper- and Lower-Plane Seismicity in Northern Chile

Intermediate-depth seismicity in northern Chile is dominated by a highly active north-south–trending belt between ~80 and 100 km depth, which is visible in both seismicity planes (Fig. 2). Upper-plane seismicity further features a prominent region of enhanced activity north of the Mejillones Peninsula below the onshore part of the seismogenic zone (A1 in Figs. 2A and 7). This feature is related to the Michilla earthquake of 16 December 2007, a M_w 6.9 event that occurred in the aftershock series of the M_w 7.7 Tocopilla earthquake. Unlike the latter, which ruptured the downdip part of the plate interface, the Michilla earthquake occurred on a vertical fault that extended from the plate interface to the oceanic Moho, effectively rupturing through the subducting oceanic crust (Fuenzalida et al., 2013). The Michilla event spawned its own aftershock series, and microseismicity levels along its fault plane have been elevated compared to the surroundings until today. In the event classification scheme of Sippl et al. (2018) that we adopt here, events occurring >3 km and <16 km below the slab surface are defined as belonging to the upper plane. This means that the aftershocks of the Michilla earthquake, which extend from the plate interface (0 km below slab surface) to the oceanic Moho (7 km below slab surface), get classified as plate-interface and upper-plane events in approximately equal parts. Besides the Michilla cluster, upper-plane seismicity updip of the highly active north-south–trending belt is relatively homogeneous, with slightly elevated event numbers in the offshore region northwest of the Mejillones Peninsula (A2 in Figs. 2 and 7) as well as in several small clusters around 20°S–21.5°S (e.g., C1 in Figs. 2 and 7). Features A1 and A2 in the region of the Mejillones Peninsula were most active in the aftershock sequence of the 2007 Tocopilla earthquake but have featured low activity rates since then (Fig. 7). Feature C1 at 21.3°S, in contrast, does not show any marked activity peaks in time but rather represents a temporally stable feature of elevated background seismicity. Downdip of this region, upper-plane seismicity inside the highly active belt decreases north of 19.5°S and south of 22.5°S. The peculiar shape of the belt is due to a large-scale discontinuity of event locations around 21.2°S, with events south of this discontinuity occurring farther down the slab. For a detailed description of this geometry, whose origin is still not well understood, the reader is referred to Sippl et al. (2018).

The distribution of lower-plane seismicity in northern Chile is more heterogeneous compared to the upper plane, including larger areas with few or no events (Fig. 2B). Between 19.0°S and 20.7°S, the lower plane updip of the active north-south–trending belt is only weakly active. The majority of lower-plane seismicity there is concentrated in the central part of the subduction zone, between segments 10 and 31 (Figs. 2 and 5). Around 21°S, a highly active patch of lower-plane events is situated under the marine forearc, at depths of 50–75 km (P1 in Fig. 2). Southeast of this patch, a second highly active structure traces the coastline at a depth of ~70–90 km, extending from 21.0°S to 22.7°S (P2 in Fig. 2). The elongated geometry of feature P2, with the long axis oriented parallel to the coast and the trench, is peculiar. Both patches were continuously active throughout the studied time period (Fig. 7). Farther downdip, the lower plane in the highly active north-south–trending belt is characterized by very high event numbers between ~20.5 and 22.5°S (Fig. 2B). The peculiar geometry of the belt including the offset at ~21.2°S is even more prominent compared to the upper plane. Moreover, the area of high event numbers in the belt is situated directly downdip of patches P1 and P2 and is separated into two parts, with the southern part displaced downdip relative to the northern one. It therefore seems to be mimicked by the two clusters farther updip. The *b*-values (Fig. 5) mainly follow the trends that are found in the seismicity distribution, with relatively homogeneous values between 0.85 and 1.05 throughout the upper plane and a higher variability of values in the lower plane. The region of elevated lower-plane seismicity between segments 20 and 30 coincides with markedly higher *b*-values (≥1) in the lower seismicity plane. Lower-plane *b*-values are quite low (≤0.7) north of segment 37, where lower-plane event numbers are low.

JAPAN TRENCH

Geologic Setting of the Japan Trench Subduction Zone

The Japan Trench subduction zone is shaped by the subduction of the Early Cretaceous Pacific plate under the Okhotsk plate (Fig. 3) (Müller et al., 2008). Convergence occurs at ~9.2 cm/a toward the northwest (DeMets et al., 2010). Adjacent to the gap between the islands of Honshu and Hokkaido, the transition from the Japan Trench to the Kuril Trench is marked by a prominent kink in trench orientation, from north-northeast (Japan Trench) to east-northeast (Kuril Trench). This particular geometry leads to more subduction obliquity offshore Hokkaido relative to Honshu and has important ramifications for slab geometry and the regional thermal structure (e.g., Wada et al., 2015). Beneath Honshu, the Pacific plate subducts in a remarkably straight geometry at an angle of ~30° until it impinges on and gets deflected by the 660-km-depth discontinuity (Tao et al., 2018). Slab dip steepens under Hokkaido toward the Kuril Islands (Syracuse et al., 2010). Intermediate-depth seismicity outlines the archetypical double seismic zone first identified by Hasegawa et al. (1978), with two separated planes of earthquakes ~25–30 km apart (Igarashi et al., 2001; Zhang et al., 2004). The double seismic zone extends to depths of ~200 km. While event density, especially in the lower plane, is variable, the double seismic zone is present along the entire length of the margin discussed here. Earthquake focal mechanisms show downdip extension in the lower and downdip compression in the upper plane of the double seismic zone (Hasegawa et al., 1978; Kawakatsu and Seno, 1983), which has been interpreted as the signature of plate unbending (Kawakatsu, 1986).

Around 36°N, the northeast-striking Joban Seamount Chain collides with the marine forearc, with Daiichi-Kashima Seamount currently located in the trench axis. The seamount chain projects into the subduction zone at ~36°N (cf. white dots in Fig. 3 for subducting linear features). Around 41°N, at the

transition from the Japan to the Kuril Trench, Erimo Seamount rises from the trench floor. A second smaller seamount has been inferred north of Erimo Seamount under the outermost marine forearc (Fig. 3; Yamazaki and Okamura, 1989). In contrast to the Daiichi-Kashima Seamount, Erimo Seamount and the subducted smaller seamount represent isolated topographic anomalies that do not belong to seamount chains. In addition to the seamounts, two prominent oceanic fracture zones are currently subducting in the study region. Around 36°N, the north-northwest–trending Kashima fracture zone intersects the Japan Trench slightly northeast of the Daiichi-Kashima Seamount. The Kashima fracture zone subducts toward the northwest under the central to northern part of Honshu. Toward the northeastern edge of the study region, the northwest-trending Nossapu fracture zone is subducting at the Kuril Trench under the northeastern edge of Hokkaido.

Sediment thickness on the oceanic plate is generally thin (<400 m) and only locally increases to ~600 m near the deformation front (Ludwig et al., 1966; Boston et al., 2014). The thin sediments allow the identification of tectonic structures on the oceanic plate along the Japan Trench. Different authors have qualitatively and/or quantitatively investigated the deformation of the Pacific plate in the trench and outer-rise region offshore Japan (Kobayashi et al., 1998; Nakanishi, 2011; Tsuru et al., 2000; Boston et al., 2014; Fujie et al., 2018). Nakanishi (2011), in his careful description of bending-related deformation, reported two main strike directions of bending-induced faults. The first group strikes parallel to the magnetic lineation (~60°–70°) and is formed by reactivated paleo-spreading fabric, whereas the second group strikes in a north-south direction and is represented by new bend faults parallel to the trench axis. However, no study has yet systematically quantified oceanic-plate faulting along the ~1000 trench kilometers from the Chiba Prefecture (Honshu) to the northeastern tip of Hokkaido.

Oceanic-Plate Faulting along the Japan Trench

The oceanic plate is dominated by two main sets of faults striking in different directions (Fig. 4B; cf. Nakanishi, 2011). The first group strikes in a north-south direction (340°–040°), which is parallel to the trench and coastline along the island of Honshu (black lines in Fig. 3). These faults dominate the tectonic setting along the Japan Trench (south of segment ~60). Oriented oblique to the magnetic lineation (~064°; Müller et al., 2008), these faults likely represent new bend faults (Nakanishi, 2011). Along the northern margin of the Joban Seamount Chain, the new bend faults are partly overprinted by faults striking 040°–080°. This strike direction is parallel to the magnetic lineation, and the faults likely represent spreading-related faults that are reactivated during plate bending (Nakanishi, 2011). The reactivation of the paleo-spreading fabric in these segments coincides with a slight deviation in the trend of the trench from approximately north-south farther to the south to NNE-SSW farther to the north. Around the transition from the Japan Trench to the Kuril Trench, the dominant strike direction of faults on the oceanic plate changes from approximately north-south (340–040°) to approximately ENE-WSW (040°–080°). North of segment 70, plate bending is solely accommodated by reactivated spreading-related faults. The cumulated (per segment) exposed fault area is highest at the southern end of the study region (segments 0–7) and between segments 45–50 (Fig. 5B). This correlates to the two regions where new bend faults represent the only active faults on the oceanic plate (Fig. 4B).

The change in fault strike direction and the regional coexistence of faults striking in multiple directions is reflected in the distribution of I nodes and X and Y nodes (Fig. 5). Along the northern margin of the Joban Seamount Chain (plate segments ~25–39), the coexistence of all three node types indicates that faults commonly intersect other faults. This is similarly observed at the transition from the Japan to the Kuril Trench, where bending-induced faulting changes from the generation of new bend faults to the reactivation of spreading-related faults. Elsewhere, the dominance of I nodes indicates the absence of fault intersections.

Upper- and Lower-Plane Seismicity along the Japan Trench Subduction Zone

Intermediate-depth seismicity along the Japan Trench subduction zone is markedly different from that along northern Chile. The two planes of the double seismic zone are located farther apart (Fig. 6), and while they gradually approach each other toward greater depths (e.g., van Keken et al., 2012), there is no sudden closure of the gap between them or a massive increase in event numbers at a certain depth like in northern Chile. The events are also shifted to larger depths compared to northern Chile, which is likely a consequence of a colder thermal regime in the older Pacific slab. Thus, our imposed cutoff at 50 km depth that was used to separate plate-interface seismicity from intraslab seismicity should not significantly truncate the distribution of lower-plane seismicity.

Upper-plane seismicity in northeastern Japan is relatively homogeneous in most places but shows three prominent regions of elevated event numbers (A1, A2, and C1 in Figs. 3A and 7). Feature A1, which exhibits the largest concentration of upper-plane seismicity, had a large peak of activity in 2003 (Fig. 7). The peak in activity corresponds to the M 7.1 Miyagi earthquake and its aftershock series (Okada and Hasegawa, 2003). This large upper-plane event ruptured a steep plane from the slab top to ~15 km below. A large part of the rupture and its aftershock sequence thus occurred between the two planes of regular background seismicity (see also Kita et al., 2010) but was apparently all mapped into upper-plane seismicity by our approach. Feature A2, located offshore Oshika Peninsula, mainly contains events from the year 2011, when the M 9.0 Tohoku earthquake triggered a population of unusually deep (50–65 km) aftershocks inside the subducting plate (Asano et al., 2011). Cluster C1, lastly, consists of two subclusters and, unlike the other two upper-plane clusters, is not caused by a single large event and its aftershock sequence,

but rather features relatively stable background seismicity during our entire observation period (Fig. 7). Beyond these features, there appears to be a consistent downdip change in upper-plane seismicity. Event numbers are highest along the coastline between the 40 and 80 km slab-surface contours (Fig. 3) at depths of ~70–90 km. This corresponds to the belt of slightly elevated event numbers in the upper plane described by Kita et al. (2006). Farther downdip, the seismicity rate appears to decay. No along-strike changes in upper-plane event numbers are visible, except for aftershock series A1 showing up as a spike of upper-plane event numbers around plate segment 40 (Fig. 5). We note a subtle increase in upper-plane event numbers across the projection of the Joban Seamount Chain but no measurable change where the Kashima fracture zone is projected (Fig. 3). Upper-plane *b*-values are likewise relatively stable along strike, varying within the interval $0.7 < b < 0.9$. The broad peak between segments 35–45 corresponds to the spike in event numbers at segment 40 (aftershock series A1); the broadening is an effect of the 11-segment moving window we used for the *b*-value computation. Its presence indicates that events in the aftershock series A1 feature a higher *b*-value than the background seismicity elsewhere in the upper seismicity plane.

For the lower plane, there are two patches with elevated activity. Feature P1 is located south of 38°N (plate segments 5–30), and P2 is located north of 42°N (segments >80; see Figs. 3 and 5). Figure 7 shows that both patches show elevated activity rates throughout the study period. In addition to the patches, there are three aftershock series (A3–A5) that exhibit activity peaks characteristic for mainshock-aftershock sequences. A small region of enhanced activity on the southwestern edge of patch P1 is nearly co-located with upper-plane cluster C1 but is rather constantly active through time and shows no abnormal event rates in 2003 when the M 7.1 Miyagi earthquake took place. Due to a larger distance between trench and shoreline and a larger spacing between the seismicity planes in northeastern Japan, lower-plane events along the coastline are situated at deeper depths compared to their counterparts in northern Chile. Lower-plane seismicity is sparsest and commences farthest from the trench around the kink in the subduction geometry between Honshu and Hokkaido. Figure 3 shows elevated event numbers in feature P1, which covers a wide region across the subducting Joban Seamount Chain and Kashima fracture zone. However, there remains considerable variation in the prominence and width of seismicity-rate anomalies around these two seafloor features at different depth levels. Lower-plane *b*-values are, as also observed in northern Chile, more variable than their upper-plane counterparts (Fig. 5B). They correlate with lower-plane seismicity activity, with high *b*-values in regions of more lower-plane events. While *b*-values of 0.8–0.95 are found south of segment 25, which corresponds to the northern flank of the Joban Seamount Chain, there is a prominent *b*-value minimum at segments 40–55 where values as low as 0.55 are obtained. North of segment 55, *b*-values range between 0.7 and 0.9. Lower-plane *b*-values along central Honshu (south of segment 30) are on average slightly higher compared to their counterparts along Hokkaido (north of segment 50; Fig. 5B), which is consistent with the findings of Kita and Ferrand (2018).

DISCUSSION

Does Intermediate-Depth Seismicity Correlate with Hydration in the Subducting Plate?

Since Kirby et al. (1996) documented a correlation between subducting features on the Nazca plate and numbers of intermediate-depth earthquakes beneath South America, it has been suspected that intermediate-depth seismicity may be quantitatively related to the hydration of the subducting plate. Barcheck et al. (2012) found no strong global correlation between intermediate-depth seismicity and the projected water content of subducting slabs. Their assumed water contents were, however, based only on slab thermal models and the mineralogy derived from these. Nowadays, there is growing evidence that the nature of oceanic-plate faulting exerts a major influence on the amount and depth of plate hydration, which is in turn correlated to earthquake activity in the subducting slab (Ranero et al., 2003; Shillington et al., 2015; Fujie et al., 2018; Boneh et al., 2019). Whether the relation between hydration and seismicity is similar for both the upper and lower planes in double seismic zones, or whether there are systematic differences between both planes, is currently not known. Previous studies have indicated that earthquakes within the upper plane are commonly homogenously distributed along a margin, whereas activity within the lower plane is commonly patchy and even absent in some regions (Igarashi et al., 2001; Kita et al., 2010; Sippl et al., 2018).

Lower-plane earthquakes are commonly associated with the dehydration of antigorite serpentinite (Peacock, 2001), which typically occurs in a narrow temperature window (600–650 °C) and largely independent of pressure conditions (Schmidt and Poli, 1998). This implies that the presence of lower-plane seismicity depends on whether some antigorite is available beyond the depth of the 600 °C isotherm. It further seems plausible that a higher amount of antigorite results in a higher amount of hydration at the isotherm, thereby inducing higher seismicity rates. There may be limitations to this relation, given that laboratory experiments have shown that the dehydration of pure antigorite is aseismic whereas antigorite dehydration in a mixture of antigorite and olivine produces acoustic emissions (Ferrand et al., 2017). In practice, however, this likely does not play a major role because pure antigorite (corresponding to complete serpentinization of the mantle) would almost never be present in a subducting slab. Even in the uppermost kilometers of lithospheric mantle, serpentinite fractions estimated from seismic wave speeds are mostly on the order of 5%–20% (e.g., Ivandic et al., 2008; Grevemeyer et al., 2018), and even for the highest available estimate of 40% for the Nicaragua subduction zone (Van Avendonk et al., 2011), it is unlikely that the abovementioned limitation would be significant.

For the upper plane of double seismic zones, the link between slab hydration and seismicity is less well understood compared to the lower plane. There is no consensus on the full range of dehydration reactions that are responsible for seismicity within this plane. It has been suggested that upper-plane events can occur in both the lowermost oceanic crust and uppermost oceanic mantle

(Abers et al., 2013). This would imply very different mineralogy and thus different sets of dehydration reactions. The comparison of event rates between upper planes of different subduction zones is therefore not necessarily meaningful. Most studies that investigated seismicity across subducting features on the oceanic plate did not differentiate between upper- and lower-plane earthquakes (Lange et al., 2010; Dzierma et al., 2012). Nakajima and Hasegawa (2006), however, found an elongated region of increased upper-plane seismicity beneath southeastern Japan, which they correlated to a subducting fracture zone. Spatial variations in slab hydration due to the subduction of oceanic features may therefore, at least under certain circumstances, influence upper-plane seismicity.

Influence of Oceanic-Plate Faulting on Upper-Plane Seismicity

Upper-plane seismicity in both subduction zones is dominated by a single margin-parallel belt of elevated event numbers. In northern Chile, the belt is located downdip of the 80 km slab isoline (Fig. 2A), whereas in Japan it trends along the coast, roughly coinciding with the 60 km slab isoline (Fig. 3A). The existence of the belt in northern Chile is not limited to the upper plane but coincides with a region where the entire upper 25–30 km of the slab becomes seismogenic (cf. profiles in Fig. 2). The active volume includes the upper plane, the lower plane, and the region in between (see profiles in Fig. 2). It possibly owes its existence to cascading dehydration reactions of previously metastable minerals (Sippl et al., 2019) at temperatures <600 °C, but the processes responsible for its generation are currently not well understood. The margin-parallel belt of elevated upper-plane activity along the Japan subduction zone (Fig. 3) has been previously recognized by Kita et al. (2006), who tentatively identified a part of the additional seismicity there as small events that occur as a consequence of volume reduction during eclogitization of the lower oceanic crust (Nakajima et al., 2013).

Apart from the belts, the upper plane in both subduction zones is rather homogeneously active, and also the *b*-values are much more homogeneous compared to the lower plane (Fig. 5). We are not able to identify a quantitative relation between the magnitude of oceanic-plate faulting and upper-plane seismicity. More faults as well as larger cumulative exposed fault areas do not appear to result in more earthquakes in the upper plane. The same holds true for the pattern of oceanic-plate faulting. Neither the reactivated spreading-related faults nor the new bend faults or the 100°–140° striking faults in Chile result in an increase in upper-plane earthquake activity or a significant change of *b*-value. Where spatially confined regions of elevated seismicity rate are observed within the upper plane, they usually relate to aftershock sequences of large intraplate earthquakes (Fig. 7). The subducting seamounts that flank the Iquique Ridge (cf. Fig. 8) do not lead to significantly increased upper-plane event numbers in northern Chile (Fig. 2). The same holds true for the Kashima fracture zone and the Joban Seamount Chain, which are subducting along the Japan Trench.

The reported persistent background activity of the upper plane complies with previous observations from both subduction zones (Igarashi et al., 2001; Sippl et al., 2018). A sufficient amount of hydration seems to be persistently reached at the respective depth of the upper plane regardless of whether the plane is located in the lowermost oceanic crust or uppermost oceanic mantle, (i.e., at 5–7 km below the seafloor). This is consistent with the ubiquity of bending-related faults in the trench and outer-rise region in both subduction zones. All oceanic plates are subject to extensional stresses when they start to bend at the outer rise, which may explain why almost all subduction zones have an upper plane of intermediate-depth seismicity. The only exceptions to this pattern occur where extremely young and thus warm oceanic plates are subducting, such as along the western North American coast, where intermediate-depth seismicity seems to be essentially absent (Bostock et al., 2019).

But why does an increase in oceanic-plate faulting not cause a systematic increase in upper-plane seismicity? This observation may be explained with temperature-dependent reaction kinetics of the reactions that bind water in hydrous mineral assemblages. While water is brought to depth along discrete fractures, the surface area of wall rock directly exposed to this water is small. Hydration reactions thus need to proceed from the fracture surfaces into the wall rock, which is a slow, diffusion-like process. Numerical modeling of serpentinization has shown that the propagation of the reaction front into the wall rock has its optimum speed at a temperature of ~270 °C (Iyer et al., 2012). Temperatures at the outer rise at 5–7 km beneath the seafloor, where the upper plane later develops, are much lower than this optimum, which implies that hydration reactions proceed significantly slower (Fig. 9). This could imply that although more faulting with intersecting faults of different orientations (Figs. 2–5) does create an extensive fracture network that promotes the infiltration of water, the sluggish reaction kinetics at low temperature prevent more water from being bound into hydrous minerals. This leads to the homogeneous appearance of upper-plane seismicity along northern Chile, Japan, and elsewhere, irrespective of the style and magnitude of faulting at the outer rise (e.g., Igarashi et al., 2001). At lower-plane depths, in contrast, the limiting factor for seismicity is not the speed of wall-rock hydration, which is much quicker due to elevated temperatures there (Peacock, 2001; Iyer et al., 2012), but the availability of water (see the next section).

Influence of Oceanic-Plate Faulting on Lower-Plane Seismicity

Earthquake activity in the lower plane stands in contrast to the largely homogeneous activity in the upper plane. Here, most of the active regions show up as persistent features over the entire observation period (Fig. 7). Furthermore, there are large regions in both subduction zones where no or only very few earthquakes are observed within the lower plane. The *b*-values of the lower plane fluctuate more compared to the upper plane, with higher values in regions of elevated seismicity (Fig. 5). Together, these observations suggest that slab hydration at lower-plane depths of ≥25 km below the slab surface is

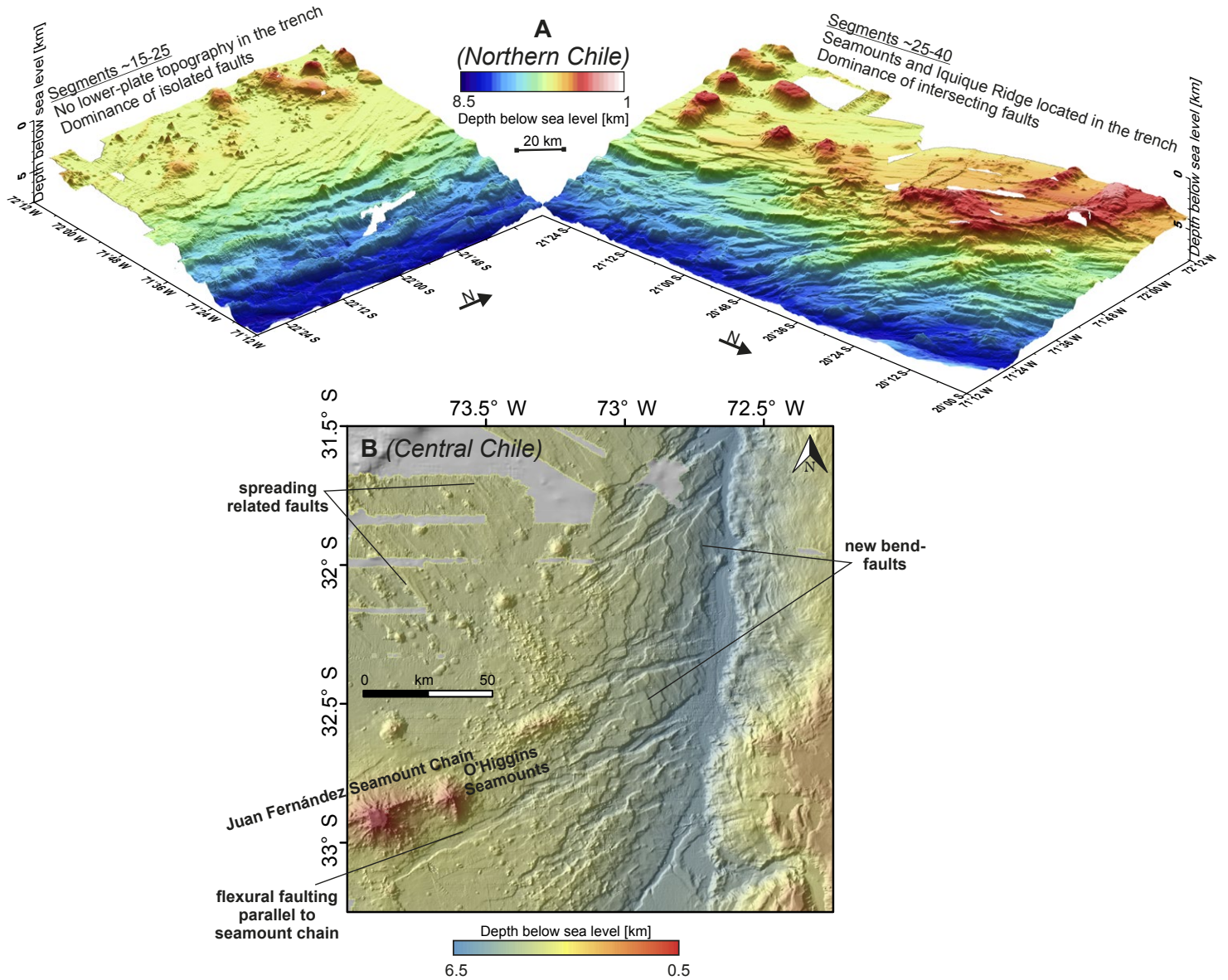

Figure 8. Detailed bathymetric maps of fault patterns in response to excess topography on the oceanic plate in the Chilean trench and outer-rise regions. (A) Three-dimensional perspective view of the oceanic Nazca plate along the northern Chilean trench, looking from the continental slope onto the outer trench wall and outer rise. Segment numbers refer to our oceanic-plate segments (see Fig. 2). (B) Seafloor morphology in the central Chilean trench in the region of the O'Higgins Seamounts. The west-east–trending seamounts are flanked by escarpments trending parallel to the seamounts that may have resulted from flexural faulting of the lithosphere along the Juan Fernández Seamount Chain. In the trench region, the coexistence of these flexural faults with new bending-induced normal faults causes the generation of a network of active intersecting faults.

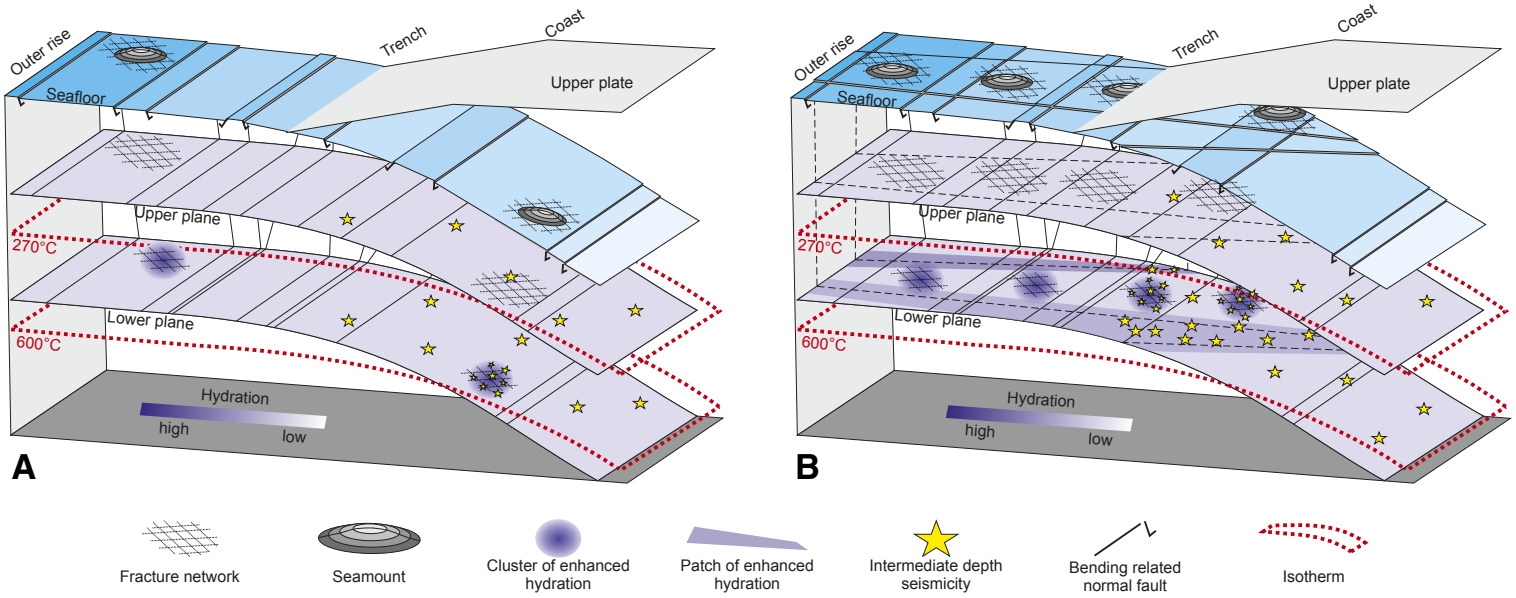

Figure 9. Conceptual model on how isolated seamounts (A) as well as groups or chains of seamounts (in this case representative for different analogues of excess topography on the oceanic plate) (B) impact faulting and hydration (prior to subduction) as well as dehydration and seismicity (during subduction) in the upper and lower planes of double seismic zones. Along the northern Chilean and Japan Trench subduction zones, upper-plane seismicity is little affected by the pattern and magnitude of oceanic-plate faulting. For the lower plane, isolated seamounts may cause localized faulting, hydration, dehydration, and seismicity as interpreted for different locations along the Japan Trench. A linear chain or a dense accumulation of seamounts, as observed for the Iquique Ridge (Chile) or the Joban Seamount Chain (Japan), can increase oceanic-plate faulting and intermediate-depth seismicity.

quite variable. Given that we observe comparable short-wavelength changes in the deformation pattern of the oceanic plates in the trench and outer-rise region, we suggest that lower-plane seismicity is substantially influenced by oceanic-plate faulting. Below, we discuss the structural and tectonic settings that may support increased localized hydration to depths beyond 25 km below the slab surface in the northern Chilean and Japan Trench subduction zones as well as elsewhere.

In northern Chile, lower-plane patch P1 is located between plate segments ~22–32 under the offshore forearc (Fig. 2). These segments show the maximum cumulative fault lengths and exposed fault areas in the trench and outer-rise region. Furthermore, they show the highest variation in fault trends and highest number of intersecting faults due to the coexistence of new bend faults and reactivated spreading-related faults. The increase in fault density and magnitude of faulting (cf. Fig. 8) may well lead to an increase in the volume of faulted and damaged rock, especially around the fault intersections (Fig. 9). Activation of the new bend faults and the reactivated spreading-related faults during large intraplate events likely enhances the circulation of water down to a depth around the 270 °C isotherm in the mantle, where serpentinization is expected to be fastest (Billen et al., 2007; Obana et al., 2012; Iyer et al., 2012).

Patch P1 further coincides with a group of at least 15 major seamounts on the oceanic plate that seem to trend along the southeastern flank of the Iquique Ridge (Fig. 8). It has been suggested that these seamounts represent the unsubducted conjugate of the Austral Plateau on the Pacific plate (Gutscher et al., 1999). This would argue for the presence of additional seamounts under the offshore forearc and coastal area of northern Chile (i.e., where patches P1 and P2 are located). The downdip continuity of these two lower-plane patches into a region of markedly increased seismicity >20 km below the slab surface inside the highly active belt of intermediate depth seismicity between 80 and 120 km depth (Fig. 2) may outline a larger-scale structure of elevated deep hydration, possibly represented by the Austral Plateau, that has been subducted over a long time scale. Elevated *b*-values within these patches further support the notion of locally increased hydration.

A linear chain of large seamounts (i.e., the Joban Seamount Chain) is also observed at the southwestern corner of the Japan Trench subduction zone. Here, the seamounts subduct at the southern edge of lower-plane patch P1 (Fig. 3). On the oceanic plate, the Joban Seamount Chain is flanked on its northern side by an ~100-km-wide zone where the coexistence of new bend faults (strike direction 340°–040°) and reactivated spreading-related faults

(strike direction 040°–080°) leads to an increase in fault intersections (X and Y nodes; Fig. 5). As a consequence, faulting is taken up equally by new bend faults and spreading-related faults. In contrast, farther to the southwest (plate segments 0–10) as well as to the northeast (segments 40–60), bending-induced deformation is almost solely accommodated by new bend faults. Projected into the subduction zone, the zone of active and intersecting faults on the northern flank of the Joban Seamount Chain correlates with a wide region of enhanced lower-plane activity (patch P1; Fig. 3).

Another observation that suggests a possible influence of subducting seamounts on lower-plane seismicity comes from the spatial extent of clusters C2 and C3 as well as several smaller clusters inside patches P1 and P2 that we do not treat individually in the Japan Trench subduction zone (Fig. 3). These clusters show a circular to elliptical shape and commonly occur rather isolated within regions of low background activity in the lower plane. The only structure that shows a comparable shape as well as wavelength of change are the seamounts on the Pacific plate (Fig. 3). Some of the seamounts near the trench, such as the Takuyo-Daisan Guyot, were created ca. 120 Ma near the Pacific superswell region (Pringle and Duncan, 1995), and the region around patch P1 and cluster C2 would also project back to the superswell in a similar time frame, ca. 120–130 Ma.

There are two mechanisms that seem plausible for causing enhanced mantle hydration around a seamount. First, in Chile as well as Japan, the seamounts are flanked by a complex network of new bend faults and reactivated spreading-related faults, leading to a high number of fault intersections. In addition to bending-related faulting parallel to the trench, flexural faulting parallel to the seamounts may further increase the magnitude of deformation and the number of fault intersections, as observed for the O'Higgins Seamounts in central Chile (Fig. 8b). Together, these may lead to an increase in the volume of faulted and damaged rock around the fault intersections and thus increased hydration of the oceanic mantle when the faults are activated (Billen et al., 2007; Obana et al., 2012) (Fig. 9). Second, it has recently been hypothesized that intraplate volcanism might create a fracture network that allows for metasomatism of the lithospheric mantle beneath the Moho (Park and Rye, 2019). The hypothesis is based on seismic observations of anisotropic, seismically slow underplated layers and anomalous swell topography beneath Hawaii and the Azores (Park and Rye, 2019). The enhanced and deep cracking near the volcanic centers is due to a combination of enhanced thermal cracking (Korenaga, 2007, 2017) owing to magmatism and/or thermal rejuvenation, metasomatic volumetric expansion (e.g., Klein et al., 2015), and/or flexural stresses induced by volcanic loading (e.g., Hieronymus and Bercovici, 2001). This hypothesis could be consistent with our bathymetric observations.

Finally, lower-plane patch P1 in the southwestern corner of the Japan Trench partly coincides with the subducting Kashima fracture zone (Fig. 3). The patch marks a broad increase in background seismicity around the fracture zone (Fig. 3), accompanied by elevated *b*-values. There is evidence that the oceanic basement around fracture zones differs from normal oceanic crust. It may be partly composed of mantle rocks that have been altered by serpentinization (Blackman et al., 1998; Sauter et al., 2013; Rüpke and Hasenclever, 2017). For the Lesser Antilles subduction zone, fracture zones have been identified as potential carriers of serpentinized oceanic mantle into the subduction zone (Schlaphorst et al., 2016; Paulatto et al., 2017; Cooper et al., 2020), although it has to be noted that these fracture zones developed in slow-spreading Atlantic crust. Increased earthquake activity in the subducting plate has been previously reported from around fracture zones in different subduction zones (e.g., Kirby et al., 1996; Lange et al., 2010; Dzierma et al., 2012). Fracture zone–induced changes in composition and alteration of the oceanic basement may lead to locally enhanced input of water (hydrated mantle minerals) into a subduction zone. While this may affect the entire subduction zone from the shallow plate boundary to large depths, the influence might be highest on the intensity of lower-plane seismicity due to the excess availability of hydrated mantle minerals. Another series of fracture zones, including the Nossapu fracture zone, is located at the northeastern corner of the Kuril Trench (Fig. 3). These fracture zones are outside the area where we could distinguish upper- and lower-plane events in the JMA earthquake catalog, thus we cannot analyze their possible seismicity signature in this manuscript.

CONCLUSIONS

From the combined analysis of high-resolution earthquake catalogs, which allow us to distinguish intermediate-depth seismicity that belongs to the upper or lower planes of double seismic zones, and high-resolution ship-based bathymetric data that allow us to map, characterize, and quantify faults on the oceanic plate prior to subduction, we draw the following conclusions:

(1) The magnitude and style of oceanic-plate faulting prior to subduction can vary significantly along a subduction zone.
(2) Increased deformation of the oceanic plate correlates to regions of enhanced earthquake activity in the lower plane of double seismic zones but is not reflected in the pattern of upper-plane seismicity.
(3) The lack of a spatial correlation between oceanic-plate faulting and upper-plane seismicity may be due to the fact that slow reaction kinetics at 5–7 km depth below the seafloor in the outer-rise region limit slab hydration despite the pervasive presence of oceanic-plate faults.
(4) To facilitate the circulation of water to mantle depths beyond 25 km, a high degree of faulting in combination with the presence of crosscutting faults that increase the volume of damaged wall rock around the faults is necessary. At these locations, enhanced hydration paves the way for an active lower plane once the hydrated mantle subducts beyond the 600–650 °C isotherm.
(5) Elevated lower-plane *b*-values correlate to regions of crosscutting faults in the outer-rise region, where enhanced hydration is inferred. These active fault networks lead to higher event numbers with a relatively larger proportion of smaller events, consistent with the hypothesis of Kita and Ferrand (2018). Whether *b*-values are systematically higher in the upper plane (as discussed by Florez and Prieto [2019]) may depend on the exact choice of the analyzed region due to a high degree of spatial variability of lower-plane *b*-values over short distances.

(6) Structural and topographic features on the oceanic plate may enhance oceanic-plate faulting and therefore modify the composition and hydration state of the surrounding mantle. Once subducted, these features are commonly characterized by a high degree of lower-plane seismicity, whereas the upper plane shows no comparable signature.

Due to the lack of high-resolution earthquake catalogues that facilitate distinguishing between the upper and lower planes of double seismic zones, our current analysis is limited to the Japan Trench and northern Chile margins. However, future improvements in the resolution of local seismicity catalogues will allow further quantification of the complex interrelation between oceanic-plate faulting, lithosphere hydration, and intermediate-depth seismicity.

ACKNOWLEDGMENTS

We acknowledge helpful discussions with T. John, M. Machek, and I. Grevemeyer. We thank the Associate Editor Philippe Agard as well as two anonymous reviewers for constructive comments that helped to improve the manuscript.

REFERENCES CITED

Abers, G.A., Nakajima, J., van Keken, P.E., Kita, S., and Hacker, B.R., 2013, Thermal-petrological controls on the location of earthquakes within subducting plates: Earth and Planetary Science Letters, v. 369–370, p. 178–187, https://doi.org/10.1016/j.epsl.2013.03.022.

Angermann, D., Klotz, J., and Reigber, C., 1999, Space-geodetic estimation of the Nazca–South America Euler vector: Earth and Planetary Science Letters, v. 171, p. 329–334, https://doi.org/10.1016/S0012-821X(99)00173-9.

Asano, Y., Saito, T., Ito, Y., Shiomi, K., Hirose, H., Matsumoto, T., Aoi, S., Hori, S., and Sekiguchi, S., 2011, Spatial distribution and focal mechanisms of aftershocks of the 2011 off the Pacific coast of Tohoku Earthquake: Earth, Planets and Space, v. 63, p. 669–673, https://doi.org/10.5047/eps.2011.06.016.

Barcheck, C.G., Wiens, D.A., van Keken, P.E., and Hacker, B.R., 2012, The relationship of intermediate- and deep-focus seismicity to the hydration and dehydration of subducting slabs: Earth and Planetary Science Letters, v. 349–350, p. 153–160, https://doi.org/10.1016/j.epsl.2012.06.055.

Beck, S.L., Zandt, G., Ward, K.M., and Scire, A., 2015, Multiple styles and scales of lithospheric foundering beneath the Puna Plateau, central Andes, *in* DeCelles, P.G., Ducea, M.N., Carrapa, B., and Kapp, P.A., eds., Geodynamics of a Cordilleran Orogenic System: The Central Andes of Argentina and Northern Chile: Geological Society of America Memoir 212, p. 43–60, https://doi.org/10.1130/2015.1212(03).

Bello-González, J.P., Contreras-Reyes, E., and Arriagada, C., 2018, Predicted path for hotspot tracks off South America since Paleocene times: Tectonic implications of ridge-trench collision along the Andean margin: Gondwana Research, v. 64, p. 216–234, https://doi.org/10.1016/j.gr.2018.07.008.

Billen, M., Cowgill, E., and Buer, E., 2007, Determination of fault friction from reactivation of abyssal-hill faults in subduction zones: Geology, v. 35, p. 819–822, https://doi.org/10.1130/G23847A.1.

Blackman, D.K., Cann, J.R., Janssen, B., and Smith, D.K., 1998, Origin of extensional core complexes: Evidence from the Mid-Atlantic Ridge at Atlantis Fracture Zone: Journal of Geophysical Research, v. 103, p. 21,315–21,333, https://doi.org/10.1029/98JB01756.

Bloch, W., John, T., Kummerow, J., Salazar, P., Krüger, O., and Shapiro, S.A., 2018a, Watching dehydration: Seismic indication for transient fluid pathways in the oceanic mantle of the subducting Nazca slab: Geochemistry Geophysics Geosystems, v. 19, p. 3189–3207, https://doi.org/10.1029/2018GC007703.

Bloch, W., Schurr, B., Kummerow, J., Salazar, P., and Shapiro, S.A., 2018b, From slab coupling to slab pull: Stress segmentation in the subducting Nazca plate: Geophysical Research Letters, v. 45, p. 5407–5416, https://doi.org/10.1029/2018GL078793.

Boneh, Y., Schottenfels, E., Kwong, K., van Zelst, I., Tong, X., Eimer, M., Miller, M.S., Moresi, L., Warren, J.M., Wiens, D.A., Billen, M., Naliboff, J., and Zhan, Z., 2019, Intermediate-depth earthquakes controlled by incoming plate hydration along bending-related faults: Geophysical Research Letters, v. 46, p. 3688–3697, https://doi.org/10.1029/2018GL081585.

Bostock, M.G., Christensen, N.I., and Peacock, S.M., 2019, Seismicity in Cascadia: Lithos, v. 332–333, p. 55–66, https://doi.org/10.1016/j.lithos.2019.02.019.

Boston, B., Moore, G.F., Nakamura, Y., and Kodaira, S., 2014, Outer-rise normal fault development and influence on near-trench décollement propagation along the Japan Trench, off Tohoku: Earth, Planets and Space, v. 66, 135, https://doi.org/10.1186/1880-5981-66-135.

Bouchon, M., Marsan, D., Jara, J., Socquet, A., Campillo, M., and Perfettini, H., 2018, Suspected deep interaction and triggering between giant earthquakes in the Chilean subduction zone: Geophysical Research Letters, v. 45, p. 5454–5460, https://doi.org/10.1029/2018GL078350.

Brudzinski, M.R., Thurber, C.H., Hacker, B.R., and Engdahl, E.R., 2007, Global prevalence of double Benioff zones: Science, v. 316, p. 1472–1474, https://doi.org/10.1126/science.1139204.

Cai, C., Wiens, D.A., Shen, W., and Eimer, M., 2018, Water input into the Mariana subduction zone estimated from ocean-bottom seismic data: Nature, v. 563, p. 389–392, https://doi.org/10.1038/s41586-018-0655-4.

Cooper, G.F., Macpherson, C.G., Blundy, J.D., Maunder, B., Allen, R.W., Goes, S., Collier, J.S., Bie, L., Harmon, N., Hicks, S.P., Iveson, A.A., Prytulak, J., Rietbrock, A., Rychert, C.A., Davidson, J.P., and the VoiLA team, 2020, Variable water input controls evolution of the Lesser Antilles volcanic arc: Nature, v. 582, p. 525–529, https://doi.org/10.1038/s41586-020-2407-5.

Coulbourn, W.T., and Moberly, R., 1977, Structural evidence of the evolution of fore-arc basins off South America: Canadian Journal of Earth Sciences, v. 14, p. 102–116, https://doi.org/10.1139/e77-011.

DeMets, C., Gordon, R.G., and Argus, D.F., 2010, Geologically current plate motions: Geophysical Journal International, v. 181, p. 1–80, https://doi.org/10.1111/j.1365-246X.2009.04491.x.

Dorbath, C., Gerbault, M., Carlier, G., and Guiraud, M., 2008, Double seismic zone of the Nazca plate in northern Chile: High-resolution velocity structure, petrological implications, and thermomechanical modeling: Geochemistry Geophysics Geosystems, v. 9, Q07006, https://doi.org/10.1029/2008GC002020.

Dzierma, Y., Rabbel, W., Thorwart, M., Koulakov, I., Wehrmann, H., Hoernle, K., and Comte, D., 2012, Seismic velocity structure of the slab and continental plate in the region of the 1960 Valdivia (Chile) slip maximum—Insights into fluid release and plate coupling: Earth and Planetary Science Letters, v. 331, p. 164–176, https://doi.org/10.1016/j.epsl.2012.02.006.

Faccenda, M., 2014, Water in the slab: A trilogy: Tectonophysics, v. 614, p. 1–30, https://doi.org/10.1016/j.tecto.2013.12.020.

Faccenda, M., Gerya, T.V., Mancktelow, N.S., and Moresi, L., 2012, Fluid flow during slab unbending and dehydration: Implications for intermediate-depth seismicity, slab weakening and deep water recycling: Geochemistry Geophysics Geosystems, v. 13, Q01010, https://doi.org/10.1029/2011GC003860.

Ferrand, T.P., 2019, Seismicity and mineral destabilizations in the subducting mantle up to 6 GPa, 200 km depth: Lithos, v. 334–335, p. 205–230, https://doi.org/10.1016/j.lithos.2019.03.014.

Ferrand, T.P., Hilairet, N., Incel, S., Deldicque, D., Labrousse, L., Gasc, J., Renner, J., Wang, Y., Green, H.W., II, and Schubnel, A., 2017, Dehydration-driven stress transfer triggers intermediate-depth earthquakes: Nature Communications, v. 8, 15247, https://doi.org/10.1038/ncomms15247.

Florez, M.A., and Prieto, G.A., 2019, Controlling factors of seismicity and geometry in double seismic zones: Geophysical Research Letters, v. 46, p. 4174–4181, https://doi.org/10.1029/2018GL081168.

Fuenzalida, A., Schurr, B., Lancieri, M., Sobiesiak, M., and Madariaga, R., 2013, High-resolution relocation and mechanism of aftershocks of the 2007 Tocopilla (Chile) earthquake: Geophysical Journal International, v. 194, p. 1216–1228, https://doi.org/10.1093/gji/ggt163.

Fujie, G., Kodaira, S., Kaiho, Y., Yamamoto, Y., Takahashi, T., Miura, S., and Yamada, T., 2018, Controlling factor of incoming plate hydration at the north-western Pacific margin: Nature Communications, v. 9, 3844, https://doi.org/10.1038/s41467-018-06320-z.

Geersen, J., 2019, Sediment-starved trenches and rough subducting plates are conducive to tsunami earthquakes: Tectonophysics, v. 762, p. 28–44, https://doi.org/10.1016/j.tecto.2019.04.024.

Geersen, J., Ranero, C.R., Barckhausen, U., and Reichert, C., 2015, Subducting seamounts control interplate coupling and seismic rupture in the 2014 Iquique earthquake area: Nature Communications, v. 6, 8267, https://doi.org/10.1038/ncomms9267.

Geersen, J., Ranero, C.R., Klaucke, I., Behrmann, J.H., Kopp, H., Tréhu, A.M., Contreras-Reyes, E., Barckhausen, U., and Reichert, C., 2018a, Active tectonics of the North Chilean marine forearc and adjacent oceanic Nazca Plate: Tectonics, v. 37, p. 4194–4211, https://doi.org/10.1029/2018TC005087.

Geersen, J., Ranero, C.R., Kopp, H., Behrmann, J.H., Lange, D., Klaucke, I., Barrientos, S., Diaz-Naveas, J., Barckhausen, U., and Reichert, C., 2018b, Does permanent extensional deformation

in lower forearc slopes indicate shallow plate-boundary rupture?: Earth and Planetary Science Letters, v. 489, p. 17–27, https://doi.org/10.1016/j.epsl.2018.02.030.
Grevemeyer, I., Ranero, C.R., and Ivandic, M., 2018, Structure of oceanic crust and serpentinization at subduction trenches: Geosphere, v. 14, p. 395–418, https://doi.org/10.1130/GES01537.1.
Gutscher, M.-A., Olivet, J.-L., Aslanian, D., Eissen, J.-P., and Maury, R., 1999, The "lost Inca Plateau": Cause of flat subduction beneath Peru?: Earth and Planetary Science Letters, v. 171, p. 335–341, https://doi.org/10.1016/S0012-821X(99)00153-3.
Hacker, B.R., 2008, H_2O subduction beyond arcs: Geochemistry Geophysics Geosystems, v. 9, Q03001, https://doi.org/10.1029/2007GC001707.
Hacker, B.R., Peacock, S.M., Abers, G.A., and Holloway, S.D., 2003, Subduction factory: 2. Are intermediate-depth earthquakes in subducting slabs linked to metamorphic dehydration reactions?: Journal of Geophysical Research, v. 108, 2030, https://doi.org/10.1029/2001JB001129.
Hainzl, S., Sippl, C., and Schurr, B., 2019, Linear relationship between aftershock productivity and seismic coupling in the northern Chile subduction zone: Journal of Geophysical Research: Solid Earth, v. 124, p. 8726–8738, https://doi.org/10.1029/2019JB017764.
Harmon, N., Rychert, C., Collier, J., Henstock, T., van Hunen, J., and Wilkinson, J.J., 2019, Mapping geologic features onto subducted slabs: Geophysical Journal International, v. 219, p. 725–733, https://doi.org/10.1093/gji/ggz290.
Hasegawa, A., Umino, N., and Takagi, A., 1978, Double-planed structure of the deep seismic zone in the northeastern Japan arc: Tectonophysics, v. 47, p. 43–58, https://doi.org/10.1016/0040-1951(78)90150-6.
Hayes, G.P., Moore, G.L., Portner, D.E., Hearne, M., Flamme, H., Furtney, M., and Smoczyk, G.M., 2018, Slab2, a comprehensive subduction zone geometry model: Science, v. 362, p. 58–61, https://doi.org/10.1126/science.aat4723.
Hieronymus, C.F., and Bercovici, D., 2001, A theoretical model of hotspot volcanism: Control on volcanic spacing and patterns via magma dynamics and lithospheric stresses: Journal of Geophysical Research, v. 106, p. 683–702, https://doi.org/10.1029/2000JB900355.
Igarashi, T., Matsuzawa, T., Umino, N., and Hasegawa, A., 2001, Spatial distribution of focal mechanisms for interplate and intraplate earthquakes associated with the subducting Pacific plate beneath the northeastern Japan arc: A triple-planed deep seismic zone: Journal of Geophysical Research, v. 106, p. 2177–2191, https://doi.org/10.1029/2000JB900386.
Ivandic, M., Grevemeyer, I., Berhorst, A., Flueh, E.R., and McIntosh, K., 2008, Impact of bending related faulting on the seismic properties of the incoming oceanic plate offshore of Nicaragua: Journal of Geophysical Research, v. 113, B05410, https://doi.org/10.1029/2007JB005291.
Iyer, K., Rüpke, L.H., Morgan, J.P., and Grevemeyer, I., 2012, Controls of faulting and reaction kinetics on serpentinization and double Benioff zones: Geochemistry Geophysics Geosystems, v. 13, Q09010, https://doi.org/10.1029/2012GC004304.
Japan Agency for Marine-Earth Science and Technology, 2016, Data and Sample Research System for Whole Cruise Information in JAMSTEC (DARWIN): http://www.godac.jamstec.go.jp/darwin/ (accessed November 2019).
John, T., Medvedev, S., Rüpke, L.H., Andersen, T.B., Podladchikov, Y.Y., and Austrheim, H., 2009, Generation of intermediate-depth earthquakes by self-localizing thermal runaway: Nature Geoscience, v. 2, p. 137–140, https://doi.org/10.1038/ngeo419.
Katsumata, A., 2010, Depth of the Moho discontinuity beneath the Japanese islands estimated by traveltime analysis: Journal of Geophysical Research, v. 115, B04303, https://doi.org/10.1029/2008JB005864.
Kawakatsu, H., 1986, Double seismic zones: Kinematics: Journal of Geophysical Research, v. 91, p. 4811–4825, https://doi.org/10.1029/JB091iB05p04811.
Kawakatsu, H., and Seno, T., 1983, Triple seismic zone and the regional variation of seismicity along the northern Honshu arc: Journal of Geophysical Research, v. 88, p. 4215–4230, https://doi.org/10.1029/JB088iB05p04215.
Kelemen, P.B., and Hirth, G., 2007, A periodic shear-heating mechanism for intermediate-depth earthquakes in the mantle: Nature, v. 446, p. 787–790, https://doi.org/10.1038/nature05717.
Kirby, S., Engdahl, E.R., and Denlinger, R., 1996, Intermediate-depth intraslab earthquakes and arc volcanism as physical expressions of crustal and uppermost mantle metamorphism in subducting slabs, *in* Bebout, G.E., Scholl, D.W., Kirby, S.H., and Platt, J.P., eds., Subduction: Top to Bottom: American Geophysical Union Geophysical Monograph 96, p. 195–214, https://doi.org/10.1029/GM096p0195.
Kita, S., and Ferrand, T.P., 2018, Physical mechanisms of oceanic mantle earthquakes: Comparison of natural and experimental events: Scientific Reports, v. 8, 17049, https://doi.org/10.1038/s41598-018-35290-x.
Kita, S., Okada, T., Nakajima, J., Matsuzawa, T., and Hasegawa, A., 2006, Existence of a seismic belt in the upper plane of the double seismic zone extending in the along-arc direction at depths of 70–100 km beneath NE Japan: Geophysical Research Letters, v. 33, L24310, https://doi.org/10.1029/2006GL028239.
Kita, S., Okada, T., Hasegawa, A., Nakajima, J., and Matsuzawa, T., 2010, Existence of interplane earthquakes and neutral stress boundary between the upper and lower planes of the double seismic zone beneath Tohoku and Hokkaido, northeastern Japan: Tectonophysics, v. 496, p. 68–82, https://doi.org/10.1016/j.tecto.2010.10.010.
Klein, F., Grozeva, N.G., Seewald, J.S., McCollom, T.M., Humphris, S.E., Moskowitz, B., Berquó, T.S., and Kahl, W.-A., 2015, Experimental constraints on fluid-rock reactions during incipient serpentinization of harzburgite: American Mineralogist, v. 100, p. 991–1002, https://doi.org/10.2138/am-2015-5112.
Klügel, A., Hansteen, T.H., van den Bogaard, P., Strauss, H., and Hauff, F., 2011, Holocene fluid venting at an extinct Cretaceous seamount, Canary archipelago: Geology, v. 39, p. 855–858, https://doi.org/10.1130/G32006.1.
Kobayashi, K., Nakanishi, M., Tamaki, K., and Ogawa, Y., 1998, Outer slope faulting associated with the western Kuril and Japan trenches: Geophysical Journal International, v. 134, p. 356–372, https://doi.org/10.1046/j.1365-246x.1998.00569.x.
Korenaga, J., 2007, Thermal cracking and the deep hydration of oceanic lithosphere: A key to the generation of plate tectonics?: Journal of Geophysical Research, v. 112, B05408, https://doi.org/10.1029/2006JB004502.
Korenaga, J., 2017, On the extent of mantle hydration caused by plate bending: Earth and Planetary Science Letters, v. 457, p. 1–9, https://doi.org/10.1016/j.epsl.2016.10.011.
Lange, D., Tilmann, F., Rietbrock, A., Collings, R., Natawidjaja, D.H., Suwargadi, B.W., Barton, P., Henstock, T., and Ryberg, T., 2010, The fine structure of the subducted Investigator Fracture Zone in western Sumatra as seen by local seismicity: Earth and Planetary Science Letters, v. 298, p. 47–56, https://doi.org/10.1016/j.epsl.2010.07.020.
Ludwig, W.J., Ewing, J.I., Ewing, M., Murauchi, S., Den, N., Asano, S., Hotta, H., Hayakawa, M., Asanuma, T., Ichikawa, K., and Noguchi, I., 1966, Sediments and structure of the Japan Trench: Journal of Geophysical Research, v. 71, p. 2121–2137, https://doi.org/10.1029/JZ071i008p02121.
Matthews, K.J., Maloney, K.T., Zahirovic, S., Williams, S.E., Seton, M., and Müller, R.D., 2016, Global plate boundary evolution and kinematics since the late Paleozoic: Global and Planetary Change, v. 146, p. 226–250, https://doi.org/10.1016/j.gloplacha.2016.10.002.
Moberly, R., Shepherd, G.L., and Coulbourn, W.T., 1982, Forearc and other basins, continental margin of northern and southern Peru and adjacent Ecuador and Chile, *in* Leggett, J.K., ed., Trench-Forearc Geology: Sedimentation and Tectonics on Modern and Ancient Active Plate Margins: Geological Society of London Special Publication 10, p. 171–189, https://doi.org/10.1144/GSL.SP.1982.010.01.11.
Müller, R.D., Sdrolias, M., Gaina, C., and Roest, W.R., 2008, Age, spreading rates, and spreading asymmetry of the world's ocean crust: Geochemistry Geophysics Geosystems, v. 9, Q04006, https://doi.org/10.1029/2007GC001743.
Nakajima, J., and Hasegawa, A., 2006, Anomalous low-velocity zone and linear alignment of seismicity along it in the subducted Pacific slab beneath Kanto, Japan: Reactivation of subducted fracture zone?: Geophysical Research Letters, v. 33, L16309, https://doi.org/10.1029/2006GL026773.
Nakajima, J., Uchida, N., Shiina, T., Hasegawa, A., Hacker, B.R., and Kirby, S.H., 2013, Intermediate-depth earthquakes facilitated by eclogitization-related stresses: Geology, v. 41, p. 659–662, https://doi.org/10.1130/G33796.1.
Nakanishi, M., 2011, Bending-related topographic structures of the subducting plate in the northwestern Pacific Ocean, *in* Ogawa, Y., Anma, R., and Dilek, Y., eds., Accretionary Prisms and Convergent Margin Tectonics in the Northwest Pacific Basin: Springer, Dordrecht, Modern Approaches in Solid Earth Sciences, v. 8, p. 1–38, https://doi.org/10.1007/978-90-481-8885-7_1.
Nakata, T., Goto, H., Watanabe, M., Suzuki, Y., Nishizawa, A., Izumi, N., Horiuchi, D., and Kido, Y., 2012, Active faults along Japan Trench and source faults of large earthquakes, *in* Proceedings of the International Symposium on Engineering Lessons Learned from the 2011 Great East Japan Earthquake, March 1–4, 2012, Tokyo, Japan: p. 254–262.
Nanjo, K.Z., Ishibe, T., Tsuruoka, H., Schorlemmer, D., Ishigaki, Y., and Hirata, N., 2010, Analysis of the completeness magnitude and seismic network coverage of Japan: Bulletin of the Seismological Society of America, v. 100, p. 3261–3268, https://doi.org/10.1785/0120100077.
Nyberg, B., Nixon, C.W., and Sanderson, D.J., 2018, NetworkGT: A GIS tool for geometric and topological analysis of two-dimensional fracture networks: Geosphere, v. 14, p. 1618–1634, https://doi.org/10.1130/GES01595.1.

Obana, K., Fujie, G., Takahashi, T., Yamamoto, Y., Nakamura, Y., Kodaira, S., Takahashi, N., Kaneda, Y., and Shinohara, M., 2012, Normal-faulting earthquakes beneath the outer slope of the Japan Trench after the 2011 Tohoku earthquake: Implications for the stress regime in the incoming Pacific plate: Geophysical Research Letters, v. 39, L00G24, https://doi.org/10.1029/2011GL050399.

Okada, T., and Hasegawa, A., 2003, The M7.1 May 26, 2003 off-shore Miyagi Prefecture Earthquake in northeast Japan: Source process and aftershock distribution of an intra-slab event: Earth, Planets and Space, v. 55, p. 731–739, https://doi.org/10.1186/BF03352482.

Ono, S., 1998, Stability limits of hydrous minerals in sediment and mid-ocean ridge basalt compositions: Implications for water transport in subduction zones: Journal of Geophysical Research, v. 103, p. 18,253–18,267, https://doi.org/10.1029/98JB01351.

Park, J., and Rye, D.M., 2019, Why is crustal underplating beneath many hot spot islands anisotropic?: Geochemistry Geophysics Geosystems, v. 20, p. 4779–4809, https://doi.org/10.1029/2019GC008492.

Paulatto, M., Laigle, M., Galve, A., Charvis, P., Sapin, M., Bayrakci, G., Evain, M., and Kopp, H., 2017, Dehydration of subducting slow-spread oceanic lithosphere in the Lesser Antilles: Nature Communications, v. 8, 15980, https://doi.org/10.1038/ncomms15980.

Peacock, S.M., 2001, Are the lower planes of double seismic zones caused by serpentine dehydration in subducting oceanic mantle?: Geology, v. 29, p. 299–302, https://doi.org/10.1130/0091-7613(2001)029<0299:ATLPOD>2.0.CO;2.

Plümper, O., Røyne, A., Magrasó, A., and Jamtveit, B., 2012, The interface-scale mechanism of reaction-induced fracturing during serpentinization: Geology, v. 40, p. 1103–1106, https://doi.org/10.1130/G33390.1.

Pringle, M.S., and Duncan, R.A., 1995, Radiometric ages of basement lavas recovered at Loen, Wodejebato, MIT, and Takuyo-Daisan Guyots, northwestern Pacific Ocean, *in* Haggerty, J.A., Premoli Silva, I., Rack, F., and McNutt, M.K., eds., Proceedings of the Ocean Drilling Program, Scientific Results, Volume 144: College Station, Texas, Ocean Drilling Program, p. 547–557, https://doi.org/10.2973/odp.proc.sr.144.033.1995.

Ramos, V.A., Cristallini, E.O., and Pérez, D.J., 2002, The Pampean flat-slab of the Central Andes: Journal of South American Earth Sciences, v. 15, p. 59–78, https://doi.org/10.1016/S0895-9811(02)00006-8.

Ranero, C.R., Morgan, J.P., McIntosh, K.D., and Reichert, C., 2003, Bending-related faulting and mantle serpentinization at the Middle America trench: Nature, v. 425, p. 367–373, https://doi.org/10.1038/nature01961.

Ranero, C.R., Villaseñor, A., Morgan, J.P., and Weinrebe, W., 2005, Relationship between bend-faulting at trenches and intermediate-depth seismicity: Geochemistry Geophysics Geosystems, v. 6, Q12002, https://doi.org/10.1029/2005GC000997.

Ranero, C.R., von Huene, R., Weinrebe, W., and Reichert, C., 2006, Tectonic processes along the Chile convergent margin, *in* Oncken, O., Chong, G., Franz, G., Giese, P., Götze, H.-J., Ramos, V.A., Strecker, M.R., and Wigger, P., eds., The Andes—Active Subduction Orogeny: Berlin, Springer, p. 91–121, https://doi.org/10.1007/978-3-540-48684-8_5.

Rüpke, L.H., and Hasenclever, J., 2017, Global rates of mantle serpentinization and H_2 production at oceanic transform faults in 3-D geodynamic models: Geophysical Research Letters, v. 44, p. 6726–6734, https://doi.org/10.1002/2017GL072893.

Rüpke, L.H., Morgan, J.P., Hort, M., and Connolly, J.A.D., 2004, Serpentine and the subduction zone water cycle: Earth and Planetary Science Letters, v. 223, p. 17–34, https://doi.org/10.1016/j.epsl.2004.04.018.

Ryan, W.B.F., Carbotte, S.M., Coplan, J.O., O'Hara, S., Melkonian, A., Arko, R., Weissel, R.A., Ferrini, V., Goodwillie, A., Nitsche, F., Bonczkowski, J., and Zemsky, R., 2009, Global Multi-Resolution Topography synthesis: Geochemistry Geophysics Geosystems, v. 10, Q03014, https://doi.org/10.1029/2008GC002332.

Saffer, D.M., and Tobin, H.J., 2011, Hydrogeology and mechanics of subduction zone forearcs: Fluid flow and pore pressure: Annual Review of Earth and Planetary Sciences, v. 39, p. 157–186, https://doi.org/10.1146/annurev-earth-040610-133408.

Sallarès, V., and Ranero, C.R., 2005, Structure and tectonics of the erosional convergent margin off Antofagasta, north Chile (23°30′S): Journal of Geophysical Research, v. 110, B06101, https://doi.org/10.1029/2004JB003418.

Sanderson, D.J., and Nixon, C.W., 2015, The use of topology in fracture network characterization: Journal of Structural Geology, v. 72, p. 55–66, https://doi.org/10.1016/j.jsg.2015.01.005.

Sanderson, D.J., and Nixon, C.W., 2018, Topology, connectivity and percolation in fracture networks: Journal of Structural Geology, v. 115, p. 167–177, https://doi.org/10.1016/j.jsg.2018.07.011.

Sauter, D., Cannat, M., Rouméjon, S., Andreani, M., Birot, D., Bronner, A., Brunelli, D., Carlut, J., Delacour, A., Guyader, V., MacLeod, C.J., Manatschal, G., Mendel, V., Ménez, B., Pasini, V., Ruellan, E., and Searle, R., 2013, Continuous exhumation of mantle-derived rocks at the Southwest Indian Ridge for 11 million years: Nature Geoscience, v. 6, p. 314–320, https://doi.org/10.1038/ngeo1771.

Scambelluri, M., Pennacchioni, G., Gilio, M., Bestmann, M., Plümper, O., and Nestola, F., 2017, Fossil intermediate-depth earthquakes in subducting slabs linked to differential stress release: Nature Geoscience, v. 10, p. 960–966, https://doi.org/10.1038/s41561-017-0010-7.

Schlaphorst, D., Kendall, J.-M., Collier, J.S., Verdon, J.P., Blundy, J., Baptie, B., Latchman, J.L., Massin, F., and Bouin, M.-P., 2016, Water, oceanic fracture zones and the lubrication of subducting plate boundaries—Insights from seismicity: Geophysical Journal International, v. 204, p. 1405–1420, https://doi.org/10.1093/gji/ggv509.

Schmidt, M.W., and Poli, S., 1998, Experimentally based water budgets for dehydrating slabs and consequences for arc magma generation: Earth and Planetary Science Letters, v. 163, p. 361–379, https://doi.org/10.1016/S0012-821X(98)00142-3.

Shillington, D.J., Bécel, A., Nedimović, M.R., Kuehn, H., Webb, S.C., Abers, G.A., Keranen, K.M., Li, J., Delescluse, M., and Mattei-Salicrup, G.A., 2015, Link between plate fabric, hydration and subduction zone seismicity in Alaska: Nature Geoscience, v. 8, p. 961–964, https://doi.org/10.1038/ngeo2586.

Sippl, C., Schurr, B., Asch, G., and Kummerow, J., 2018, Seismicity structure of the northern Chile forearc from >100,000 double-difference relocated hypocenters: Journal of Geophysical Research: Solid Earth, v. 123, p. 4063–4087, https://doi.org/10.1002/2017JB015384.

Sippl, C., Schurr, B., John, T., and Hainzl, S., 2019, Filling the gap in a double seismic zone: Intraslab seismicity in Northern Chile: Lithos, v. 346, 105155, https://doi.org/10.1016/j.lithos.2019.105155.

Strasser, M., Kopf, A., Abegg, F.W., Asada, M., Bachmann, A.K., Cuno, P., Dos Santos Ferreira, C., Fleischmann, T., Fujiware, T., Hatakeyama, E., Heesemann, B.R., Hillman, J.I.T., Hoehne, M., Huusmann, H., Ikari, M., Ikehara, K., Jaeger, F.D., Kanamatsu, T., Kang, M.-H., Kaul, N.E., Kioka, A., Koelling, M., Lange, K., Luebben, N., Matthiessen, T., Mchugh, C.M., Meier, A., Menapace, W., Mochizuki, K., Moernaut, J., Molenaar, A.W., Moore, G.F., Mu, L.-J., Nakano, Y., Pieper, M.; Rex, M.L.P.A., Roesner, A., Schwestermann, T., Sun, T., Szczucinski, W., Toechterle, P., Truetner, S., Usami, K., Wiemer, G., and Yamaguchi, A., 2017, Report and preliminary results of R/V *SONNE* cruise SO251, Extreme events Archived in the Geological Record of Japan's Subduction margins (EAGER-Japan): Leg A SO251-1, Yokohama–Yokohama, 04.10.2016–15.10.2016; Leg B SO251-2, Yokohama–Yokohama, 18.10.2016–02.11.2016: Berichte aus dem MARUM und dem Fachbereich Geowissenschaften der Universität Bremen 318, 217 p., http://publications.marum.de/id/eprint/3677.

Syracuse, E.M., van Keken, P.E., and Abers, G.A., 2010, The global range of subduction zone thermal models: Physics of the Earth and Planetary Interiors, v. 183, p. 73–90, https://doi.org/10.1016/j.pepi.2010.02.004.

Tao, K., Grand, S.P., and Niu, F., 2018, Seismic structure of the upper mantle beneath eastern Asia from full waveform seismic tomography: Geochemistry Geophysics Geosystems, v. 19, p. 2732–2763, https://doi.org/10.1029/2018GC007460.

Tsuru, T., Park, J.O., Takahashi, N., Kodaira, S., Kido, Y., Kaneda, Y., and Kono, Y., 2000, Tectonic features of the Japan Trench convergent margin off Sanriku, northeastern Japan, revealed by multichannel seismic reflection data: Journal of Geophysical Research, v. 105, p. 16,403–16,413, https://doi.org/10.1029/2000JB900132.

Van Avendonk, H.J.A., Holbrook, W.S., Lizarralde, D., and Denyer, P., 2011, Structure and serpentinization of the subducting Cocos plate offshore Nicaragua and Costa Rica: Geochemistry Geophysics Geosystems, v. 12, Q06009, https://doi.org/10.1029/2011GC003592.

van Keken, P.E., Hacker, B.R., Syracuse, E.M., and Abers, G.A., 2011, Subduction factory: 4. Depth-dependent flux of H_2O from subducting slabs worldwide: Journal of Geophysical Research, v. 116, B01401, https://doi.org/10.1029/2010JB007922.

van Keken, P.E., Kita, S., and Nakajima, J., 2012, Thermal structure and intermediate-depth seismicity in the Tohoku-Hokkaido subduction zones: Solid Earth, v. 3, p. 355–364, https://doi.org/10.5194/se-3-355-2012.

von Huene, R., Weinrebe, W., and Heeren, F., 1999, Subduction erosion along the North Chile margin: Journal of Geodynamics, v. 27, p. 345–358, https://doi.org/10.1016/S0264-3707(98)00002-7.

Wada, I., He, J., Hasegawa, A., and Nakajima, J., 2015, Mantle wedge flow pattern and thermal structure in Northeast Japan: Effects of oblique subduction and 3-D slab geometry: Earth and Planetary Science Letters, v. 426, p. 76–88, https://doi.org/10.1016/j.epsl.2015.06.021.

Warren, L.M., Hughes, A.N., and Silver, P.G., 2007, Earthquake mechanics and deformation in the Tonga-Kermadec subduction zone from fault plane orientations of intermediate- and

deep-focus earthquakes: Journal of Geophysical Research, v. 112, B05314, https://doi.org/10.1029/2006JB004677.

Wiemer, S., and Wyss, M., 2000, Minimum magnitude of completeness in earthquake catalogs: Examples from Alaska, the western United States, and Japan: Bulletin of the Seismological Society of America, v. 90, p. 859–869, https://doi.org/10.1785/0119990114.

Wolery, T.J., and Sleep, N.H., 1976, Hydrothermal circulation and geochemical flux at mid-ocean ridges: The Journal of Geology, v. 84, p. 249–275, https://doi.org/10.1086/628195.

Yamazaki, T., and Okamura, Y., 1989, Subducting seamounts and deformation of overriding forearc wedges around Japan: Tectonophysics, v. 160, p. 207–229, https://doi.org/10.1016/0040-1951(89)90392-2.

Yamasaki, T., and Seno, T., 2003, Double seismic zone and dehydration embrittlement of the subducting slab: Journal of Geophysical Research, v. 108, 2212, https://doi.org/10.1029/2002JB001918.

Yuan, X., Sobolev, S.V., Kind, R., Oncken, O., Bock, G., Asch, G., Schurr, B., Graeber, F., Rudloff, A., Hanka, W., Wylegalla, K., Tibi, R., Haberland, C., Reitbrock, A., Giese, P., Wigger, P., Röwer, P., Zandt, G., Beck, S., Wallace, T., Pardo, M., and Comte, D., 2000, Subduction and collision processes in the Central Andes constrained by converted seismic phases: Nature, v. 408, p. 958–961, https://doi.org/10.1038/35050073.

Yuan, X., Sobolev, S.V., and Kind, R., 2002, Moho topography in the central Andes and its geodynamic implications: Earth and Planetary Science Letters, v. 199, p. 389–402, https://doi.org/10.1016/S0012-821X(02)00589-7.

Zhan, Z., 2020, Mechanisms and implications of deep earthquakes: Annual Review of Earth and Planetary Sciences, v. 48, p. 147–174, https://doi.org/10.1146/annurev-earth-053018-060314.

Zhang, H., Thurber, C.H., Shelly, D., Ide, S., Beroza, G.C., and Hasegawa, A., 2004, High-resolution subducting-slab structure beneath northern Honshu, Japan, revealed by double-difference tomography: Geology, v. 32, p. 361–364, https://doi.org/10.1130/G20261.2.